

AN ABSTRACT OF THE THESIS OF

Reyixiati Repukaiti for the degree of Master of Science in Materials Science presented on November 6, 2017.

Title: Corrosion Resistance of Alloys in Seawater and Supercritical Carbon Dioxide Environments

Abstract approved:

Julie Tucker

The corrosion resistances of several alloys were investigated to optimize performance and cost in seawater and supercritical CO₂ environments. Many alloys are prone to corrosion in seawater and/or supercritical CO₂ containing impurity environments. Exposure and electrochemical experiments were conducted in both environments to evaluate alloys' corrosion resistance. In seawater corrosion tests, salt fog spray test was conducted on 12 alloys to down select alloys with good corrosion resistance; alloy hardness in annealed and hardened conditions were considered as well. Cyclic polarization and electrochemical impedance spectroscopy were conducted to evaluate down selected alloys' corrosion resistance in different heat treatment conditions. Alloy with high Cr and Ni content generally have higher corrosion resistance, and heat treatment of alloys have negatively affected alloys' corrosion resistance. In supercritical CO₂ environments with O₂ and H₂O impurities, high pressure and temperature autoclave exposure tests were conducted to evaluate the corrosion resistance of 347H stainless steel and P91 martensitic-ferritic steel. Electrochemical

tests at ambient pressure at 25°C and 50°C were performed with H₂O saturated with CO₂ to calculate corrosion rates of the steels. X-ray diffraction and scanning electron microscopy were used to characterize corrosion products before and after corrosion testing. This study revealed that 347H has higher corrosion resistance than P91 due to higher Cr content and severe corrosion occurred during the condensation of H₂O during the shutdown period of autoclave tests.

©Copyright by Reyixiati Repukaiti

November 6, 2017

All Rights Reserved

Corrosion Resistance of Alloys in Seawater and Supercritical Carbon Dioxide
Environments

by
Reyixiati Repukaiti

A THESIS

submitted to

Oregon State University

in partial fulfillment of
the requirements for the
degree of

Master of Science

Presented November 6, 2017
Commencement June 2018

Master of Science thesis of Reyixiati Repukaiti presented on November 6, 2017

APPROVED:

Major Professor, representing Materials Science

Head of School of Mechanical, Industrial and Manufacturing Engineering

Dean of the Graduate School

I understand that my thesis will become part of the permanent collection of Oregon State University libraries. My signature below authorizes release of my thesis to any reader upon request.

Reyixiati Repukaiti, Author

ACKNOWLEDGEMENTS

I would first like to thank my major advisor, Dr. Julie Tucker, for her guidance, support, and mentorship throughout graduate school. I would also like to thank Dr. Burkan Isgor, Dr. Ömer Doğan, and Dr. Margaret Ziomek-Moroz for their excellent teaching and advice on these projects.

This research effort was performed in support of the U.S. Department of Energy, National Energy Technology Laboratory's ongoing research in Corrosion of Heat Exchanger Alloys in Supercritical Carbon Dioxide for power cycle applications.

I would like to acknowledge and thank the following people from the National Energy Technology Laboratory for their help and discussion: Dr. Dr. Nicholas Huerta, and Dr. Randal Thomas, Dr. Richard Oleksak, Dr. John Baltrus, and Mr. Jefrery Oberfoell.

I appreciate all the discussions with Dr. Xijia Lu, Mr. David Freed, and Mr. Brock Forrest of 8 Rivers Capital, which gave us insights and directions of supercritical CO₂ power cycles.

Thank you to all my friends, especially all my lab mates who helped and supported me since I joined the nuclear metallurgy and materials group.

Last, but not least, I would like to deeply thank my parents and sister for providing endless support and love.

CONTRIBUTION OF AUTHORS

Mr. Lucas Teeter, Mr. Pratik Murkute, and Mr. Cody Fast, for their help on experimental works.

Dr. Julie Tucker, Dr. Burkan Isgor, Dr. Ömer Doğan, and Dr. Margaret Ziomek-Moroz for their advice and guidance on these two projects.

TABLE OF CONTENTS

	<u>Page</u>
1. Introduction.....	1
1.1 References	5
2. Literature Review.....	6
2.1 Background	6
2.1.1 Forms of Corrosion	9
2.1.2 Corrosion Testing Methods.....	13
2.2 Salt Water Corrosion.....	17
2.3 Supercritical CO ₂ Corrosion.....	22
2.3.1 Allam Cycle	24
2.3.2 Corrosion of SCO ₂	25
2.4 References.....	30
3. Investigation of Corrosion Resistance for Annealed and Hardened Stainless Steels.....	32
3.1 Abstract.....	32
3.2 Introduction	32
3.3 PHASE 1: Preliminary Investigation	33
3.3.1 Experimental Procedure.....	35
3.3.2 Preliminary Investigation Results.....	38
3.4 PHASE 2: Corrosion Resistance Investigation of Selected Alloys in Different Heat Treatment.....	40
3.4.1 Materials and methods	40
3.4.2 Heat treatment.....	42
3.4.3 Electrochemical Test Results.....	43
3.5 Conclusion.....	46
3.6 References	46
4 Corrosion Behavior of Steels in Supercritical CO ₂ for Power Cycle Applications	48
4.1 Abstract	48
4.2 Introduction	48

TABLE OF CONTENTS (Continued)

	<u>Page</u>
4.3 Experimental Procedures.....	50
4.3.1 Autoclave Exposure Experiments.....	50
4.3.2 Electrochemical experiments	52
4.4 Results and Discussion.....	53
4.4.1 Autoclave Exposure Experiments Results	53
4.4.2 Electrochemical experiments results.....	56
4.5 Conclusions	59
4.6 Acknowledgments	60
4.7 References	61
5 Conclusion	63
5.1 Investigation of Corrosion Resistance for Annealed and Hardened Stainless Steels	64
5.2 Corrosion Behavior of Steels in Supercritical CO ₂ for Power Cycle Applications	64
6 Suggested Future works	65
6.1 Investigation of Corrosion Resistance for Annealed and Hardened Stainless Steels	65
6.2 Corrosion Behavior of Steels in Supercritical CO ₂ for Power Cycle Applications	65

LIST OF FIGURES

<u>Figure</u>	<u>Page</u>
Figure 2.1 A simple electrochemical cell [4].....	7
Figure 2.2 Schematic corrosion experimental setup [7]	15
Figure 2.3 Fe-H ₂ O Pourbaix Diagram [4].....	21
Figure 2.4 Comparison of various power cycle efficiency	23
Figure 2.5 CO ₂ phase diagram [14]	24
Figure 2.6 SCO ₂ Allam cycle diagram [15].....	25
Figure 2.7 Concentration as functions of pressure and temperature (a) <i>H₂CO₃</i> , (b) <i>HCO₃⁻</i> , (c) <i>CO₃²⁻</i>	28
Figure 2.8 Potential-pH-temperature diagram for Fe-CO ₂ -H ₂ O systems; cFe ²⁺ = 1 ppm, pCO ₂ = 1 bar.	30
Figure 3.1 Test samples in the corrosion chamber	36
Figure 3.2 Hardness data of candidate alloys	37
Figure 3.3 Corrosion performance in salt spray test: (a) M390 alloy before exposure, (b) M390 alloy after 4 days of exposure, (c) ELMAX alloy before exposure, (b) ELMAX alloy after 4 days of exposure	39
Figure 3.4 Schematic electrochemical test cell.....	41
Figure 3.5 Bode plots (impedance and phase angle) for (a) 15-5 (b) 17-7 (c) 2205 stainless steels	44
Figure 3.6 Cyclic polarization plots for (a) 15-5 (b) 17-7 (c) 2205 stainless steels ...	45
Figure 3.7 Cyclic polarization data for (a) annealed alloys (b) heat-treated alloys	46
Figure 4.1 Microstructures of candidate alloys.....	50
Figure 4.2 Autoclave experiments setup [4]	52
Figure 4.3 Temperature-pressure profile of condition 2 and 3.	52
Figure 4.4 pH measurement of electrolyte at 25 and 50°C.....	53
Figure 4.5 Mass change comparison as a function of phases at 50°C and 80 bar in condition 1.	54

LIST OF FIGURES (Continued)

<u>Figure</u>	<u>Page</u>
Figure 4.6 Mass change comparison of condition 2 and 3, as a function of Water condensation at 245°C and 80 bar in CO ₂ rich phase	55
Figure 4.7 P91 coupon images after autoclave exposure experiments	56
Figure 4.8 Potentiodynamic polarization scans	57
Figure 4.9 347H linear polarization resistance	57
Figure 4.10 P91 linear polarization resistance	57
Figure 4.11 Cyclic voltammetry scan	58
Figure 4.12 Potentiostatic polarization scan	58

LIST OF TABLES

<u>Table</u>	<u>Page</u>
Table 2.1 EMF series of metals [4].....	8
Table 2.2 Galvanic series in seawater [5]	12
Table 2.3 Ion compositions in seawater of salinity 35.....	20
Table 3.1 Chemical composition (wt. %) of alloys investigated in Phase 1.....	34
Table 3.2 Experiment duration in salt spray tests.....	38
Table 3.3 Corrosion test results	40
Table 4.1 Chemical composition of alloys	50
Table 4.2 Exposure conditions.....	51
Table 4.3 Glancing angle XRD results of corrosion products	55
Table 4.4 Corrosion rates	59

1. Introduction

Corrosion is a result of chemical or electrochemical reactions between material(s) and its environment(s) [1], and it is a severe issue that results in great economic cost and can have negative impacts on people's safety. In 2013, the global cost of corrosion was approximately \$2.5 trillion, which was 3.4% of 2013's global GDP [2]. From bridges to power plants, one small corrosion issue could cause hundreds of people's lives. A corrosion issue caused a gas pipeline explosion took 62 people's lives and injured 136 in China [3]. Therefore, reducing the corrosion phenomenon can have a positive impact for both safety and economic concerns.

Corrosion can occur in many environments, however, seawater and coastal environments are the most common. Corrosion in marine applications and structures near seawater, such as bridges and watercrafts, present economical and public safety challenges. Every year, the global cost of marine corrosion is estimated from \$50 to \$80 billion [4]. Seawater corrosion has been studied for a long period of time, and many new stainless steels are invented to prevent salt water corrosion under ambient pressure and temperature [5]. As new alloys have been developed in last few decades, a study with a variety of alloys is needed to evaluate the corrosion resistance of them and setup a baseline for comparing seawater corrosion resistance for different types of alloys. Furthermore, a balance between cost, performance, and corrosion resistance is needed, in order to optimize the lifetime of alloys for seawater applications.

Opposed to seawater corrosion as a common corrosion issue, supercritical CO₂ (SCO₂) corrosion has been gaining interest in last few years. Due to its excellent thermodynamic efficiencies, nontoxic properties, and low cost, SCO₂ is proposed as working fluid in various power cycles, such as fossil and solar power plants [6]. However, there is little corrosion data in SCO₂ due to the relatively short time these applications have existed. Impurities and varying temperature and pressure are always concerns in SCO₂, including in heat exchangers of power cycles. Heat exchangers contain post combustion products, mostly CO₂, H₂O, and O₂, and they have large temperature and pressure gradients [7]. All of these conditions with large gradient are driving forces of corrosion in heat exchangers, which is a key part of power cycles. Therefore, studies on candidate alloys with various operating conditions and impurity levels are needed to understand and predict the corrosion behaviors of materials in SCO₂ environment.

For both seawater and SCO₂ corrosion, alloy selection is a critical decision. For each application and environment, alloy selection must balance cost and performance to ensure the product properties are sustainable over its lifetime. Corrosion resistance is a fundamental factor that helps guide alloy selections. From the perspective of economy, corrosion resistance is directly linked with the price of alloys. Alloys with good corrosion resistance are typically more expensive due to higher content of Ni, Cr, etc.

Generally, three types of corrosion tests can be categorized, laboratory tests, field tests, and service tests [5]. Laboratory tests are often used to accelerate corrosion reactions

and simulate service conditions, and are often used in research, such as this thesis. A variety of methods exist within the category of laboratory tests. For instance, immersion test, spray exposure test, electrochemical test, etc. Exposure and electrochemical tests are the methods that were used in this thesis. Exposure tests are a practical way to evaluate alloys' corrosion resistance by exposing alloys in the desired environments for a length of time. Corrosion products usually can be visually observed after the tests to allow for qualitative ranking. Thus, exposure tests can give us a direct feedback of alloys' corrosion behavior in the application environment. Corrosion products and corrosion rates can also be evaluated and calculated. As an alternative, electrochemical tests can assess and control the corrosion of alloys in a different way by monitoring the corrosion behaviors, and the results can be interpreted to understand the corrosion mechanisms and corrosion rates. Both exposure and electrochemical test methods are useful for investigating seawater corrosion and SCO_2 corrosion, and the results of each test can be compared to evaluate the corrosion resistance of candidate alloys.

The purpose of this thesis is to compare the corrosion response of candidate alloys for seawater and SCO_2 applications. The thesis is organized as follows: Chapter 2 provides background information on corrosion with an emphasis on salt water and SCO_2 corrosion. Chapter 3 focuses on corrosion of multi-tool alloys in salt water environments. It is a conference proceeding that was published in *Electrochemical Society Transaction* 2017 77.11. The title of the paper is "Investigation of Corrosion

Resistance for Annealed and Hardened Stainless Steels”. The content of the paper includes:

- Objectives of salt water corrosion tests
- Phase 1: Preliminary investigation of 12 alloys
 - Materials and exposure test
 - Results and discussion
- Phase 2: Corrosion Resistance Investigation of Selected Alloys in Different Heat Treatment
 - Materials and Electrochemical test
 - Results and discussion
- Conclusion

Chapter 4 is focused on alloys for SCO_2 power plant applications. It is a published conference proceeding in Electrochemical Society Transaction 2017 77.11 as well. The title of the paper is “Corrosion Behavior of Steels in Supercritical CO_2 for Power Cycle Applications”. The content of the paper includes:

- Objectives of SCO_2 corrosion tests
- Experimental procedures of exposure and electrochemical tests
- Results and discussion
 - Exposure test weight change data
 - Corrosion rate calculation from electrochemical tests
- Conclusion

Chapter 5 presents conclusions based on these research activities to evaluate corrosion behavior of steels in various environments. Chapter 6 discusses potential future work on these topics.

1.1 References

- [1] Denny A. Jones, Principles and prevention of corrosion. New York : Toronto : New York: Macmillan PubCo; Collier Macmillan Canada ; Maxwell Macmillan International PubGroup, 1991.
- [2] “Internation Cout Of Justice: Order On Request For The Indication Of Provisional Measures In Case Concerning Application Of The Convention On The Prevention And Punishment Of The Crime Of Genocide (Bosnia And Herzegovina v. Yugoslavia (Serbia And Montenegro)),” International Legal Materials, vol. 32, no. 3, pp. 888–902, 1993.
- [3] Y. Zhu, X.-M. Qian, Z.-Y. Liu, P. Huang, and M.-Q. Yuan, “Analysis and assessment of the Qingdao crude oil vapor explosion accident: Lessons learnt,” Journal of Loss Prevention in the Process Industries, vol. 33, pp. 289–303, 2015.
- [4] Koch Gh, Brongers Mph, Thompson Ng, Virmani Yp, and Payer Jh, “Corrosion Cost and Preventive Strategies in the United States.” 2002.
- [5] K. A. Chandler, Marine and Offshore Corrosion: Marine Engineering Series. Elsevier, 2014.
- [6] S. Sarrade et al., “Overview on corrosion in supercritical fluids,” The Journal of Supercritical Fluids, vol. 120, pp. 335–344, 2017.
- [7] S. Wright, T. Conboy, and Rochau, 2011 University Turbine Systems Research Workshop, “Overview of Supercritical CO2 Power Cycle Development,” Columbus, OH (2011).

2. Literature Review

2.1 Background

Corrosion has been identified as a natural process since the Bronze Age [1], and has been identified as an electrochemical reaction since 1800s [2]. Corrosion is a study that focuses on chemical and electrochemical behavior of materials on their surfaces, and it occurs in various forms. Generally, corrosion has been defined as a negative term of materials degradation, which is true in many cases, such as rusting and degrading of steels. However, not all reactions would degrade materials. Sometimes, a healthy and protective layer needs to be formed on a surface to prevent material degradation. In this thesis, corrosion is an unwanted phenomenon that occurred and has been investigated in two studies, seawater and SCO_2 with impurities corrosion.

Traditionally, corrosion is categorized into dry and wet corrosion [3]. Dry corrosion occurs when no aqueous phase appears in the environment, and the environment usually is gaseous at an elevated temperature. Wet corrosion usually involves an aqueous phase, which creates electrochemical reactions in the system. Generally, metallic corrosion processes happen in aqueous solutions. Although dry and wet corrosion have different environments, they share similar evaluation and characterizing methodologies. This thesis mainly focuses on wet corrosion.

The nature of wet corrosion is essentially electrochemistry, which has four components: anode, cathode, electrolyte, and metallic connection, as shown in Figure 2.1 [4]. Two electrodes are submerged in an aqueous solution, and a metallic wire connects these two electrodes. The two electrodes are anode and cathode, and the solution is the electrolyte. Metallic wire allows electrons to flow from anode to cathode, and the ions can move freely in the electrolyte.

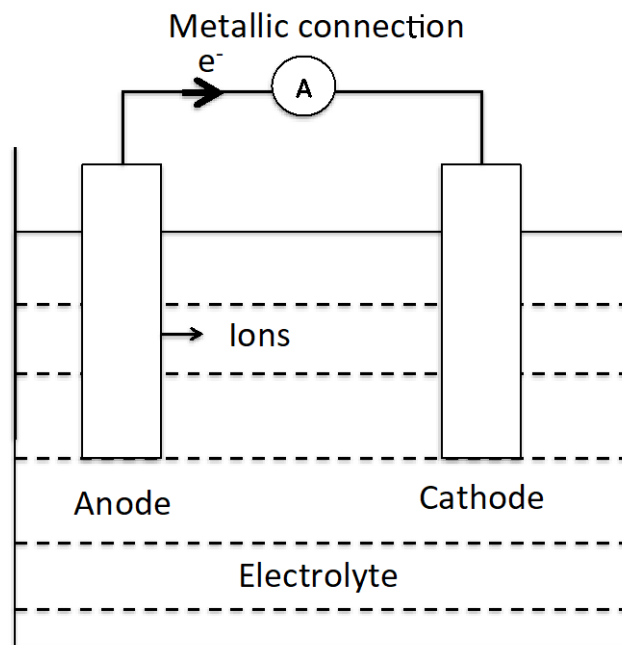


Figure 2.1 A simple electrochemical cell [4]

The roles of anode and cathode are determined by the thermodynamics of the materials in an electrochemical system. When two dissimilar metals are coupled in an electrolyte, one of them will be anode while the other one is cathode. Cathode is the electrode at which the reduction occurs, and anode is the electrode at which oxidation occurs [5]. A theoretical guide, the Standard Equilibrium Potential (EMF series, Table 2.1 [4]) versus standard hydrogen electrode (SHE), for determining anode and cathode of

metals can be followed. In the EMF series, the metal with higher potential will be the cathode when it is paired with a lower potential metal. The electrolyte determines the environment of anode and cathode. Ions can travel freely in aqueous electrolyte, typically in wet corrosion. Metallic connection is needed to complete a circuit for electrons to travel from anode to cathode. An electrochemical cell must have all 4 components to complete a corrosion process, which allows anodic electrode to corrode while cathode electrode is protected.

Table 2.1 EMF series of metals [4]

Metal	Equilibrium	E (V vs. SHE)
Gold	$\text{Au}^{3+}(\text{aq}) + 3\text{e}^{-} \rightleftharpoons \text{Au}$	1.5
Silver	$\text{Ag}^{+}(\text{aq}) + \text{e}^{-} \rightleftharpoons \text{Ag}$	0.799
Mercury	$\text{Hg}_2^{3+}(\text{aq}) + 2\text{e}^{-} \rightleftharpoons 2\text{Hg}$	0.789
Copper	$\text{Cu}^{2+}(\text{aq}) + 2\text{e}^{-} \rightleftharpoons \text{Cu}$	0.337
Hydrogen	$\text{H}^{+}(\text{aq}) + \text{e}^{-} \rightleftharpoons \frac{1}{2}\text{H}_2$	0.000
Lead	$\text{Pb}^{2+}(\text{aq}) + 2\text{e}^{-} \rightleftharpoons \text{Pb}$	-0.126
Tin	$\text{Sn}^{2+}(\text{aq}) + 2\text{e}^{-} \rightleftharpoons \text{Sn}$	-0.136
Nickel	$\text{Ni}^{2+}(\text{aq}) + 2\text{e}^{-} \rightleftharpoons \text{Ni}$	-0.250
Cadmium	$\text{Cd}^{2+}(\text{aq}) + 2\text{e}^{-} \rightleftharpoons \text{Cd}$	-0.403
Iron	$\text{Fe}^{2+}(\text{aq}) + 2\text{e}^{-} \rightleftharpoons \text{Fe}$	-0.440
Chromium	$\text{Cr}^{3+}(\text{aq}) + 3\text{e}^{-} \rightleftharpoons \text{Cr}$	-0.74
Zinc	$\text{Zn}^{2+}(\text{aq}) + 2\text{e}^{-} \rightleftharpoons \text{Zn}$	-0.763
Titanium	$\text{Ti}^{2+}(\text{aq}) + 2\text{e}^{-} \rightleftharpoons \text{Ti}$	-1.63
Aluminum	$\text{Al}^{3+}(\text{aq}) + 3\text{e}^{-} \rightleftharpoons \text{Al}$	-1.66
Magnesium	$\text{Mg}^{2+}(\text{aq}) + 2\text{e}^{-} \rightleftharpoons \text{Mg}$	-2.37

2.1.1 Forms of Corrosion

Corrosion has various forms, such as uniform corrosion, galvanic corrosion, crevice corrosion, pitting corrosion, environmentally induced cracking, hydrogen damage, intergranular corrosion, dealloying, and erosion corrosion [3]. Each corrosion form has its unique mechanism, but they are also related to each other. Thus each type of corrosion can occur individually, but usually multiple corrosion behaviors occur simultaneously. Uniform corrosion, galvanic corrosion, and pitting corrosion are relevant to this thesis and will be described in detail.

Uniform corrosion is a commonly expected corrosion type. A uniform layer of corrosion products can be formed on exposed surfaces. For example, iron oxides are common corrosion layers from iron-based alloys, typically they can be scraped off on exposed surfaces. However, uniform corrosion requires a uniform surface, which is difficult to achieve in industries. Most surfaces have pits, cracks, and/or scratches, and they would cause other types of corrosion. Furthermore, uniform corrosion desires a uniform metallurgical and compositional surface, especially for steels and alloys. Alloys usually have 5 to 10 different elemental additions, which need homogenization to have uniform chemical, physical, and mechanical properties. Uniform corrosion is a basic form of corrosion in many situations, but it mostly happens with other types of corrosion due to imperfection of surface and materials.

Galvanic corrosion is another common corrosion type. It happens when two dissimilar alloys are coupled together in an environment with electrolyte. One of the alloys would preferentially corrode, while the other alloy would be protected. A galvanic series is created in order of corrosion potential to compare alloys corrosion resistance in seawater condition in Table 2.2 [5]. The table shows that stainless steel alloys and nickel-based alloys are generally more corrosion resistance than other types of alloys [5] in seawater. This finding can be derived from the chemical compositions of the alloys with good corrosion resistance. Generally, chromium and nickel contents play an important role in corrosion resistance. Galvanic corrosion is much more obvious when two dissimilar alloys have large corrosion potential difference. This phenomenon can be applied for sacrificial anodes method, which uses an alloy with lower potential to corrode, in order to protect the other higher potential alloy.

Table 2.2 Galvanic series in seawater [5]

Cathodic
↑
Platinum
Gold
Graphite
Titanium
Silver
Zirconium
AISI Type 316, 317 stainless steel (passive)
AISI Type 304 stainless steel (passive)
AISI Type 430 stainless steel (passive)
Nickel (passive)
Copper-nickel (70-30)
Bronzes
Copper
Brasses
Nickel (active)
Naval brass
Tin
Lead
AISI type 316, 317 stainless steels (active)
AISI type 304 stainless steel (active)
Cast iron
Steel or iron
Aluminum alloy 1100
Zinc
Magnesium and magnesium alloys
↓
Anodic

Pitting corrosion is a type of localized corrosion. It is a common corrosion behavior among stainless steels. Stainless steels are made of various components, such as chromium, nickel, molybdenum, etc. All of these components contribute to form a protective passive film, chromium oxide layer is the primary protective film [6]. However, pitting corrosion occurs once the film has breakdowns, which is similar to the mechanism of crevice corrosion. Pitting corrosion happens when the alloys encounter attracting agents, such as chlorides, because chlorides can breakdown the passive film and initiate pitting corrosion. The formation of pits is usually unpredictable, and the pitting area is small. Chlorides are a common compounds in seawater, which make pitting corrosion a common corrosion behavior for stainless steels in seawater environment.

2.1.2 Corrosion Testing Methods

Corrosion of alloys is often studied in laboratories to simulate real life corrosion environments. Exposure and electrochemical tests are common ways to evaluate materials' corrosion behaviors. Exposure tests can directly provide information about the corrosion products. Corrosion products can be further characterized to understand corrosion mechanisms. Furthermore, corrosion rates can be calculated by mass loss or thickness change from materials. Electrochemical tests are generally conducted from the perspective of electrochemistry as the nature of corrosion. Electrochemical tests are able to provide and validate thermodynamics and kinetics of corrosion mechanisms. Corrosion rates and corrosion products, if any, are analyzed as well.

Exposure tests are usually accelerated environmental corrosion simulations. The results of the test can be used to compare materials' corrosion resistance, but they do not completely represent materials' corrosion behavior in real world. Specimens are exposed in a certain temperature, pressure, humidity, solution concentration, etc. for a certain duration. After exposure, the specimens can be directly compared by visual inspection and weight change. Corrosion rate of materials can be calculated from mass loss via Equation 2.1 [6],

$$\text{Corrosion Rate} \left[\frac{\text{mm}}{\text{year}} \right] = \frac{87.6 W}{DAT} \quad \text{Eq. 2.1}$$

Where:

W = weight loss [mg];

D = density [g/cm³];

A = exposed area [cm²];

T = time [hours].

Electrochemical testing is a complex and useful method to evaluate a materials' corrosion behavior. It is typically conducted in a corrosion cell with a potentiostat, as shown in Figure 2.4 [7]. A corrosion cell consists three electrodes, working, counter, and reference electrode. Working electrode is the anode, and it is the specimen electrode with an exposed surface. Counter electrode is the cathode, and usually it is an inert or noble material that does not have electrochemical or chemical reaction in the electrolyte, common materials are graphite and platinum. Reference electrode measures the potential and current of working electrode. Some common reference

electrodes are standard hydrogen electrode, saturated calomel electrode, and silver silver-chloride electrode. All three electrodes are connected to a potentiostat, which should be able to control the potential of ongoing electrochemical tests. The potentiostat that were used in the studies of the thesis are from Gamry Instruments. A variety of testing methods were used to evaluate the materials' corrosion behaviors in this thesis. Some common methods are open circuit potential, linear polarization resistance, potentiodynamic polarization, cyclic polarization, electrochemical impedance spectroscopy, etc. Much information can be gathered from conducting different types of experiments, such as corrosion rate, solution resistivity, corrosion potential and current, etc.

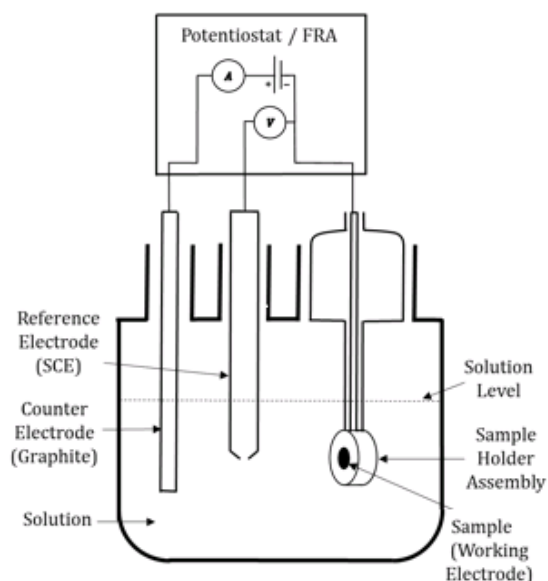


Figure 2.2 Schematic corrosion experimental setup [7]

Open circuit potential (OCP) is a free corrosion potential measurement. It is the potential change between working electrode and reference electrode. OCP gives basic information of alloys, such as nobility. Potentiodynamic polarization scan is a

destructive direct current electrochemistry technique [8]. A potential range is given prior to the scan, and then the working electrode will experience cathodic or anodic reactions. From the results of potentiodynamic polarization scan, working electrode's pitting susceptibility, corrosion potential and current, and passivity can be acquired [8]. Cyclic polarization is similar to potentiodynamic polarization scan. Cyclic polarization is a complete scan of the given potential range from the lowest to highest potential, and then goes back to the lowest potential, and it gives additional information of materials' localized corrosion susceptibility. Electrochemical impedance spectroscopy (EIS) is an alternated current method way of applying a certain frequency with small sinusoidal perturbation [8]. EIS measures the response and impedance in a given frequency range. The results of EIS contain two plots, Bode and Nyquist plots. Bode plot provides information of phase angle and impedance change as a function of frequency. Nyquist plot does not explicitly state frequency, but it shows individual charge transfer [8]. EIS also has a modelling function that can be used to model the electrochemical process as an equivalent circuit.

Corrosion rate can be calculated from the following equation (Equation 2.2) [9],

$$\text{Corrosion Rate} \left[\frac{\text{mm}}{\text{year}} \right] = K \frac{i_{\text{corr}}}{\rho} \text{EW} \quad \text{Eq. 2.2}$$

Where:

$K = 0.00327$ [mm g/ μA cm yr];

$\rho = \text{density}$ [g/cm³];

EW = equivalent weight;

i_{corr} = corrosion current density [$\mu\text{A}/\text{cm}^2$];

ρ and EW are determined from materials physical and chemical properties. i_{corr} is dependent on polarization resistance, which can be determined either from linear polarization resistance with a small potential step, typically ± 10 mV, or an approximation from potentiodynamic polarization scan near corrosion potential [9].

2.2 Seawater Corrosion

Seawater corrosion is an issue for alloys that are used in marine applications and coastline environments. Conventionally, alloys are required to have good corrosion resistance and mechanical properties in these environments. An investigation of corrosion resistance and mechanical properties of alloys in simulated seawater environment are presented in Chapter 3. In this study, alloys' corrosion resistance and hardness were compared to different heat treatments.

Various materials were used in this study, such as stainless steels, duplex stainless steels, precipitation hardened alloys, and nickel-based alloys. The selection of alloys has four criteria: corrosion resistance, mechanical properties, fabrication, and cost. Corrosion resistance varies in different environments [10]. For example, pH, temperature, pressure, humidity, etc. are the factors that influence alloys' corrosion resistance. Thus selecting the appropriate alloys with good corrosion resistance for a certain condition is the initial step. Mechanical properties do not have as large variance as corrosion resistance. However, stress corrosion cracking may occur in harsh

environments. Fabrication determines the application of alloys, such as shape, surface finish, weldability, etc. Cost is always a concern from the perspective of selecting materials. Especially for stainless steels, stainless steels with similar properties could have drastically price change due to the chemical composition difference. All of these materials have good corrosion resistance and mechanical properties at ambient temperature and pressure, which is the environment of daily-use tools.

Stainless steels are commonly used in many industries, such as kitchenware, marine applications, and power plants. Stainless steels are defined as “stainless” is because their good corrosion resistance. Stainless steels have the minimum of 11% Cr [10], and approximately 10 to 15 other elements, such as C, Ni, Mo, Co, etc. A protective Cr rich oxide layer will form on the surface when stainless steels are exposed in air. The Cr rich oxide is a passive film that prevents the base metal from further corroding. However, the protection of the Cr rich oxide layer is weak [10] when the Cr content is around 10.5%, and then localized corrosion could occur due to the breakdown of the passive layer.

Other elements can help to form and stabilize the Cr oxide layer in stainless steels and possibly enhance mechanical properties. Ni is a key element, which can increase the stability of austenitic structure, thus strengthen the mechanical properties; also, nickel has effects of reforming the passive Cr layer if it was broken [10]. Therefore, high Ni content alloys are commonly used in high temperature and pressure environment. C is a critical element, it is effective of increasing the hardness of alloys, but reducing the

toughness once the content reaches an extent; carbon and chromium reactions have negative effects on corrosion resistance by forming carbides in Cr-rich oxide layer [10]. Overall, C is beneficial for enhancing the hardness of alloys, but the composition should be controlled in order to maintain the corrosion resistance and toughness. Mo can also increase the corrosion resistance by bonding with Cr to stabilize the initiation of Cr rich oxide layer, and decrease the possibility of localized corrosion [10].

Duplex stainless steels are a two-phase alloy with approximately equal content of austenitic and ferritic microstructures. They have higher mechanical strength than austenitic stainless steels, but the corrosion resistance is similar to austenitic stainless steels. Ni-based alloys are common materials used in high temperature and pressure environments due to their high corrosion resistance and mechanical strength, thus they are effective against stress corrosion cracking [10]. Precipitation hardened alloys are stainless steels that can be hardened by aging at an elevated temperature. The hardening mechanism is achieved by adding elements to form intermetallic precipitates [10]. Corrosion resistance of precipitation hardened alloys are comparable to austenitic stainless steels.

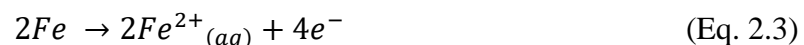
Seawater corrosion is a common phenomenon in marine and offshore environments, and alloys used in the vicinity of coastal lines often suffer from this type of corrosion. Seawater is the major source and cause of salt water corrosion. The ion compositions in seawater of salinity 35 (the concentration of dissolved salt in water) are listed in Table 2.3 [4]. The major ions are Na^+ , and Cl^- , which compose NaCl. Other cations

exist in seawater besides Na^+ , such as K^+ and Mg^{2+} . Cl^- is a major anion in seawater, and it is an attack agent to breakdown protective passive film, and it will cause localized corrosion, such as pitting and crevice corrosion [3]. The temperature of seawater varies from -2 to 35°C on worldwide, and it changes in different seasons [4]. Dissolved gases are also a factor of seawater, such as O_2 and CO_2 , and the gas saturation varies by the depth of water, thus the composition of seawater is affected by the amount of dissolved gas and the depth of seawater. pH is another concern that affects the seawater condition; seawater pH is normally between 8.1 and 8.3 as an alkaline environment, but it varies with the depth and other impurities of the environment. According to all of the uncertain factors, seawater condition is complex, and it is difficult to determine the exact condition of an alloy application's environment. In order to simplify and conduct an accelerated seawater corrosion test, using high purity NaCl solution became a popular way to evaluate alloys' corrosion resistance in laboratories [4].

Table 2.3 Ion compositions in seawater of salinity 35

Ions	Na	Mg	Ca	K	Sr	Cl	SO_4	Br	H_3BO_3
wt%	30.68	3.70	1.17	0.96	0.03	55.19	7.72	0.19	0.07

The alloys that are discussed in Chapter 3 are stainless steel, duplex stainless steel, nickel-based alloys, and precipitation hardened alloys. The major anodic reaction (Eq. 2.3) that happens for these alloys is dissolution of Fe, and the major cathodic reaction (Eq. 2.4) is oxygen reduction [4]. The standard condition Pourbaix diagram of iron-water is shown in Figure 2.3 [4]. The figure demonstrates that the major corrosion product is Fe_2O_3 when pH is around 7.



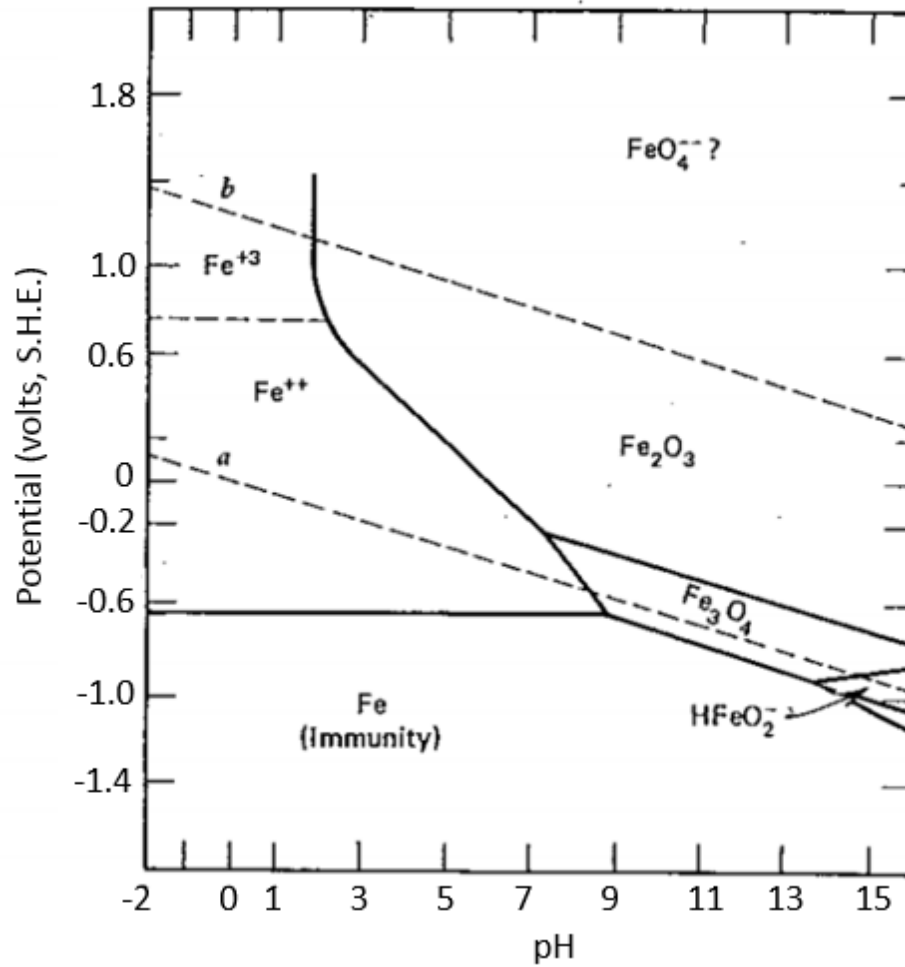


Figure 2.3 Fe-H₂O Pourbaix Diagram [4]

In an aerated NaCl solution, it has dissolved oxygen. The amount of dissolved oxygen in aerated solution decreases as salinity increases [3-5], but the corrosion rate of Fe increases until the NaCl concentration reaches approximately 3.5% due to the increasing conductivity of the solution [4]. While the Cl⁻ concentration increases, Fe²⁺ does not react immediately with OH⁻ at anodes surfaces, instead, the ions diffuses into the solution and form Fe(OH)₂ away from the surface, thus Fe(OH)₂ is not a protective layer, which allows more dissolved oxygen achieve cathodic reaction [4]. Although the

solubility of oxygen decreases as NaCl concentration increases, Cl^- provides more conductivity, the cathodic reaction reaches its peak speed before NaCl concentration reaches 3.5%. However, once the NaCl concentration is higher than 3.5%, the decreasing oxygen solubility becomes the dominant factor that slows down the cathodic reaction [4].

2.3 Supercritical CO_2 Corrosion

In 2009, the International Energy Agency (IEA) published the first Carbon Capture and Storage (CCS) roadmap, since then, reducing CO_2 emission has been widely and deeply researched worldwide. In 2013, IEA updated the CCS roadmap with the past development and future directions. Seven key actions were discussed in the 2013 CCS roadmap, reduce the cost of electricity and increase efficiency in power generation cycles was one of the actions that need to be completed in next few years [11]. Specifically, IEA calls the installation of supercritical technology on all new combustion power plants.

Supercritical technology, particularly supercritical fluids, has been researched and implemented to be a media in power cycles. H_2O and CO_2 are the popular supercritical fluids that has been drawing attention. Figure 2.4 [12] explains the reason. CO_2 Brayton Cycles and Rankine Cycles (water as supercritical fluid) have higher efficiency once the temperature is above 375°C . Thus, CO_2 and steam are widely used as heat transfer media in heat exchangers of power cycles. However, using steam as heat exchanging media usually causes severe corrosion issues when aqueous H_2O phase appears, which

establishes an electrochemical corrosion environment. Therefore, using CO₂ as a supercritical fluid has a promising future in power cycles.

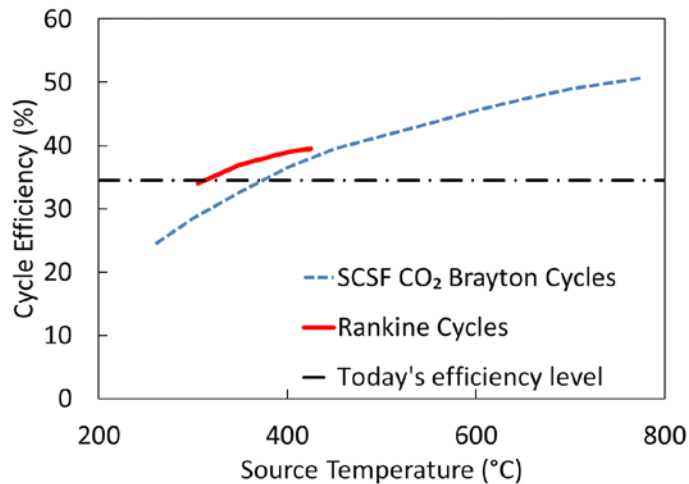


Figure 2.4 Comparison of various power cycle efficiency

Carbon dioxide usually exist in gaseous phase at room temperature and ambient pressure, or in solid phase when frozen at ambient pressure, or in liquid phase by pressurizing at room temperature [13]. Supercritical state is a phase that exist at a pressure and temperature beyond a fluid's critical point, the critical point is 31°C and 74 bar for CO₂ [14], as shown in Figure 2.5 [14]. SCO₂ can achieve similar density as liquid CO₂ by controlling the pressure, and it can be hundreds times higher than gaseous CO₂ [13]. SCO₂ has same viscosity value with gaseous CO₂, but the diffusion coefficient is 1% of gas and 100 times higher than liquid [13].

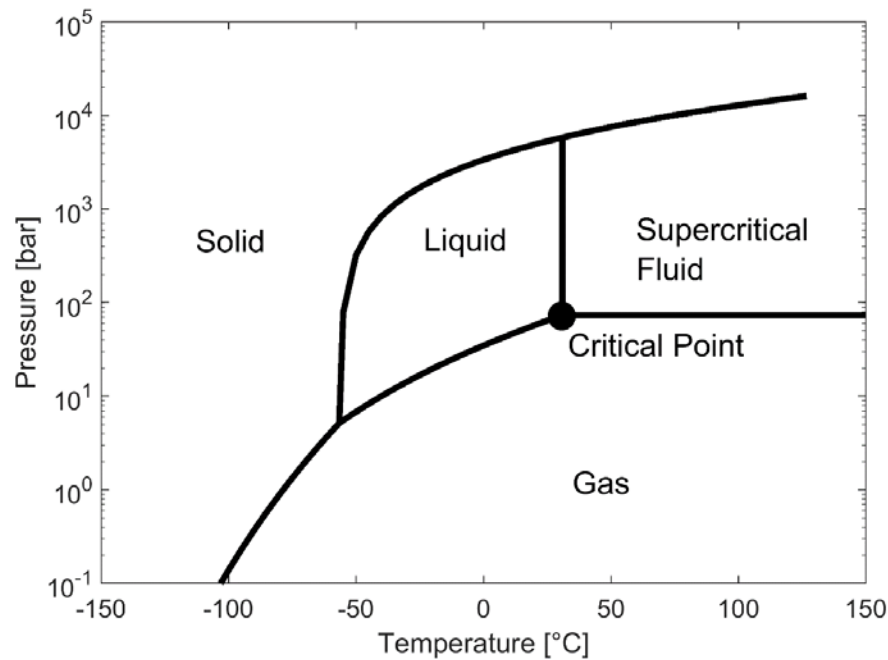


Figure 2.5 CO₂ phase diagram [14]

2.3.1 Allam Cycle

The Allam Cycle is a process that converts fossil fuels into electric power, and uses SCO₂ as a working fluid in the cycle with nearly zero CO₂ emission [15]. As shown in Figure 2.6 [15], The Allam Cycle starts from an air separation unit by extracting pure oxygen. Pure oxygen and fuel, such as natural gas, are combusted in a combustor, which provides energy to drive the CO₂ turbine to generate power. The combustion products, mainly CO₂ and H₂O, go through heat exchanger from high temperature to low temperature at a low pressure, meanwhile, the aqueous water is separated from the cycle. The rest of the combustion products goes through another cooling process to thoroughly cool down. Then high purity CO₂ is isolated into sequestration pipeline. The last CO₂ and H₂O go back to the heat exchanger from low temperature to high temperature at a high pressure, and then travel back to combustor eventually.

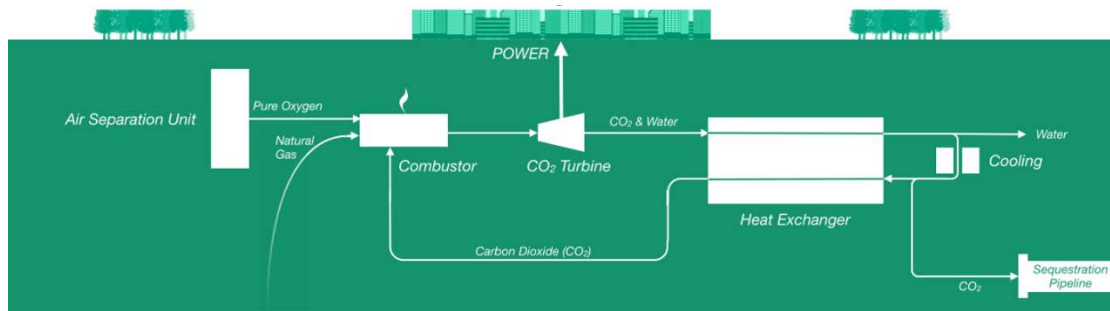


Figure 2.6 SCO₂ Allam cycle diagram [15]

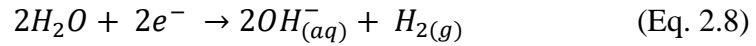
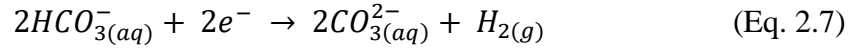
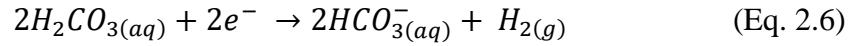
During the entire cycle, CO₂ and H₂O are the major products with little O₂ that cannot be ignored. Due to the fact that the environment has a high pressure and temperature gradient, the phase change of CO₂ and H₂O has significant impact on thermodynamic efficiency and corrosion behavior of the alloys that were used to build the cycle. The largest gradient of pressure and temperature occur in the heat exchangers. Normally, Allam Cycle has multiple heat exchangers to reduce or increase temperature and pressure gradually to ensure the lifetime of each heat changers. However, the corrosion issue still exist in the heat exchangers.

2.3.2 Corrosion of SCO₂

2.3.2.1 Water Saturated SCO₂ corrosion

Corrosion mechanisms of alloys in water saturated SCO₂ includes electrochemical reactions, chemical reactions, and mass transfer phenomena [18]. Electrochemical reactions are mainly discussed here. The electrochemical corrosion mechanism of steel alloys with CO₂ is affected by many factors, such as pH, temperature, pressure, and flow rate of CO₂. The major electrochemical reactions are listed below [18].

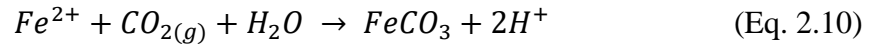
Cathodic reactions:



Anodic reactions



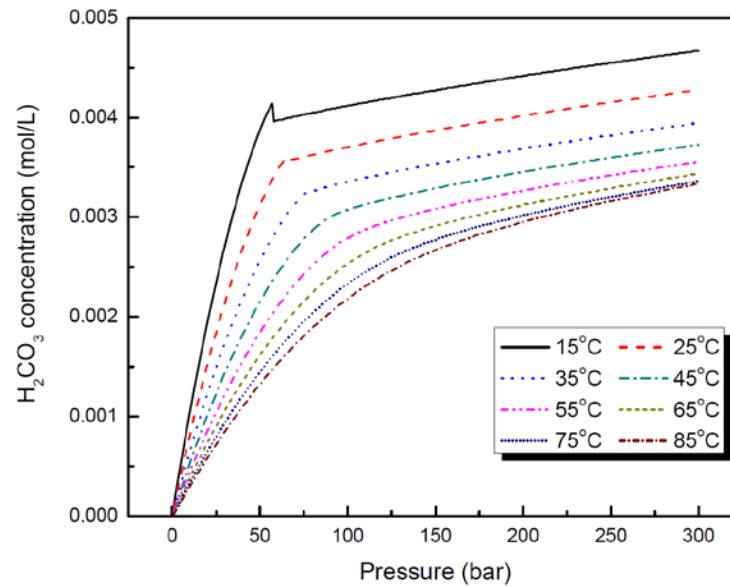
Overall reactions:



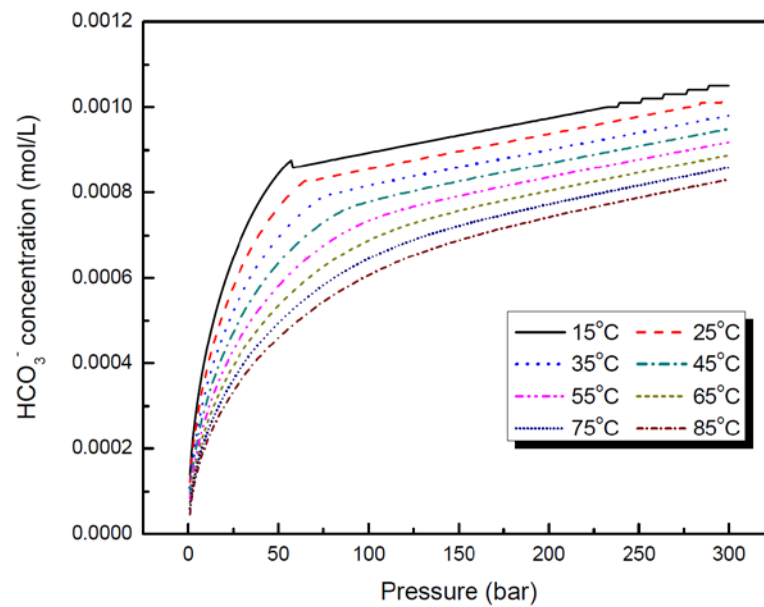
The formation of $FeCO_3$ is an important factor to determine the corrosion rate of ferrous alloys. $FeCO_3$ can be protective layer if the formation rate is faster than corrosion rate; otherwise, $FeCO_3$ would be a porous layer and non-protective layer [18].

Comparing water saturated SCO_2 with dry SCO_2 , the condition has changed from SCO_2 rich phase to H_2O rich phase [13]. Adding water into the system introduces carbonic acid, which is a weak corrosive acid. Additionally, carbonic acid can generate HCO_3^- and CO_3^{2-} as shown in equations 2.6 to 2.8. Choi *et al.* have concluded the concentrations of H_2CO_3 , HCO_3^- , and CO_3^{2-} as functions of temperature and pressure, as shown from Figure 2.7 [19]. From the figures, one can conclude that H_2CO_3 has the highest concentration among the ions in any condition; the concentration of H_2CO_3 , HCO_3^- , and CO_3^{2-} increase as pressure increases; when temperature increases, the concentration of H_2CO_3 and HCO_3^-

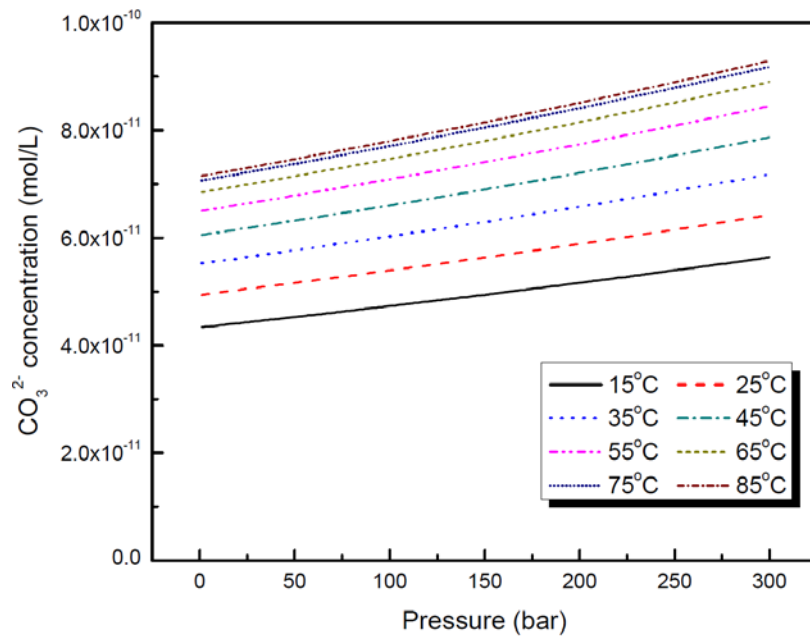
decrease, but CO_3^{2-} shows increasing concentration. From the studies of Wei et al. and Choi et al., water rich phase has significant higher corrosion rate than SCO_2 rich phase for carbon steels, and same trend were observed for stainless steels [1].



(a)



(b)



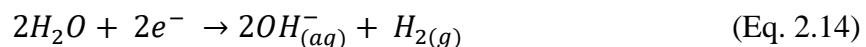
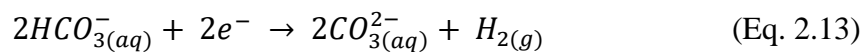
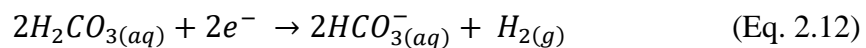
(c)

Figure 2.7 Concentration as functions of pressure and temperature (a) H_2CO_3 ,
(b) HCO_3^- , (c) CO_3^{2-}

2.3.2.2 Water Saturated SCO_2 with O_2

Allam cycle post combustion products are mainly CO_2 and H_2O , but O_2 also exists as a common impurities. Electrochemical reactions of iron alloys in water saturated SCO_2 with O_2 are listed below [20].

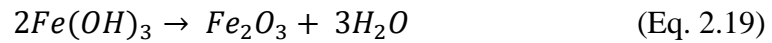
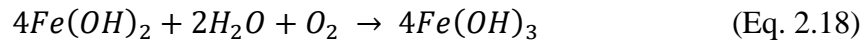
Cathodic reactions:



Anodic reactions:



Overall reactions



Tang *et al.*, Wei *et al.*, and Tanupabrungsun have concluded that O₂ plays a significant role in alloys' corrosion behaviors in water saturated SCO₂, especially for carbon steels [13, 18, 20]. With O₂, alloy corrosion rate is much higher than without O₂. O₂ induces Fe²⁺ film to form, and Fe²⁺ will be continually oxidized into Fe³⁺ or Fe₃O₄. Previously discussed, FeCO₃ could be protective layer when FeCO₃ kinetics speed is faster than the corrosion rate without O₂ in the system. However, the formation of and Fe³⁺ oxides would inhibit the formation of FeCO₃ and accelerate the Fe_(s) dissolution. Furthermore, Fe²⁺ oxides are porous and non-protective layers, and easy to flake, which exacerbate the corrosion behaviors. Tanupabrungsun has created a Pourbaix diagram of iron in water saturated SCO₂ with O₂ system as shown in Figure 2.8; it can be concluded that the major corrosion products are Fe₂O₃, Fe₃O₄, and FeCO₃, and the amount of dissolved Fe²⁺ increases at lower pH [18].

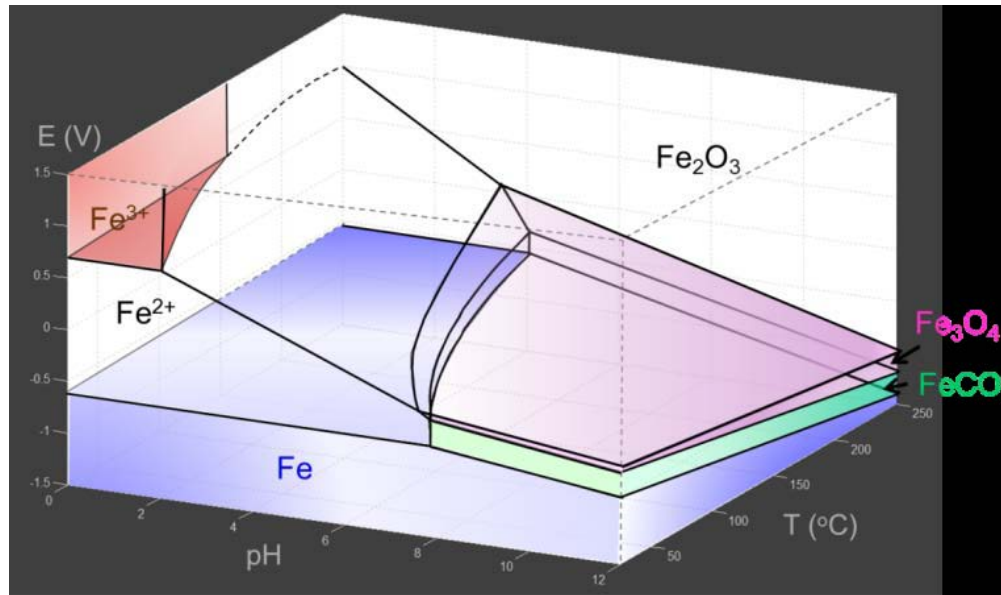


Figure 2.8 Potential-pH-temperature diagram for Fe-CO₂-H₂O systems; $c_{\text{Fe}^{2+}} = 1$ ppm, $p_{\text{CO}_2} = 1$ bar.

2.4 References

- [1] G. L. Fox, "Cupreous metal corrosion at a Bronze Age coastal marine archaeological site: a study of site processes at Tel Nami, Israel," *International Journal of Nautical Archaeology*, vol. 23, no. 1, pp. 41–47, 1994.
- [2] Frankenthal, R P. "A brief history of corrosion science and its place in the electrochemical society." *Corrosion Science: a retrospective and current status in honor of Robert P. Frankenthal*, in the Centennial Electrochemical Society Meeting (held in Philadelphia, PA, USA. 2002
- [3] Marcus, Philippe, ed. *Corrosion mechanisms in theory and practice*. Crc Press, 2011.
- [4] K. A. Chandler, *Marine and Offshore Corrosion: Marine Engineering Series*. Elsevier, 2014.
- [5] H. H. Uhlig and R. W. Revie, *Corrosion and corrosion control*. Third edition. John Wiley and Sons, Inc, New York, NY, 1985.
- [6] D. A. Jones, *Principles and prevention of corrosion*. New York : Toronto : New York: Macmillan PubCo; Collier Macmillan Canada ; Maxwell Macmillan International PubGroup, 1991.
- [7] Ghods, P., et al., Microscopic investigation of mill scale and its proposed effect on the variability of chloride-induced depassivation of carbon steel rebar. *Corrosion Science*, 2011. 53(3): p. 946-954.
- [8] Instruments, Gamry. "Basics of electrochemical impedance spectroscopy." G. Instruments, *Complex impedance in Corrosion*(2007): 1-30.
- [9] ASTM G102-89. "Standard Practice for Calculation of Corrosion Rates and Related Information from Electrochemical Measurements." Reapproved 1999.

- [10] D. Joseph R., ed. Stainless steels. ASM international, 1994.
- [11] IEA, "Technology Roadmap: Carbon Capture and Storage 2013." 2013.
- [12] S. Wright, T. Conboy, and Rochau, Overview of Supercritical CO₂ PowerCycle Development, presented at the 2011 University Turbine Systems Research Workshop, Columbus, Ohio, Oct-2011
- [13] L. Wei, Y. Zhang, X. Pang, and K. Gao, "Corrosion behaviors of steels under supercritical CO₂ conditions," Corrosion Reviews, vol. 33, no. 3–4, pp. 151–174, 2015.
- [14] NIST, "Carbon Dioxide" NIST WebBook. [Online]. Available: <http://webbook.nist.gov>. (Accessed: March 2017)..
- [15] "NetPower Technology." [Online]. Available: <https://netpower.com/technology>. [Accessed: 1-Aug-2017].
- [16] Y. S. Choi, and S. Nešić. National Association of Corrosion Engineers, "Corrosion Behavior of Carbon Steel in Supercritical CO₂ - Water Environments." Houston, TX (2009).
- [17] J. Beck, M. Fedkin, S. Lvov, M. Ziomek-Moroz, G. Gordon, and J. Tylczak, "Electrochemical System to Study Corrosion of Metals in Supercritical CO₂ Fluids," 13.
- [18] T. Tanupabrungrun, "Thermodynamics and Kinetics of Carbon Dioxide Corrosion of Mild Steel at Elevated Temperatures," Ph.D. Dissertation, Dept. Chem. Biomolecular Eng., the Russ College of Engineering and Technology of Ohio University, Athens, OH, 45701
- [19] Y.-S. Choi and S. Nestic, "Corrosion Behavior of Carbon Steel in Supercritical CO₂ - Water Environments," 22.
- [20] Y. Tang, X. P. Guo, and G. A. Zhang, "Corrosion behaviour of X65 carbon steel in supercritical-CO₂ containing H₂O and O₂ in carbon capture and storage (CCS) technology," Corrosion Science, vol. 118, pp. 118–128, 2017.

3. Investigation of Corrosion Resistance for Annealed and Hardened Stainless Steels

3.1 Abstract

Stainless steels are desirable for their good corrosion resistance and mechanical properties, and are widely used in marine applications that require high hardness. Heat treatment procedures increase the hardness of stainless steel, and affect microstructural, compositional and surface properties of these materials, hence affect their corrosion resistance. To investigate these relationships, a series of electrochemical, corrosion resistance, and mechanical tests at room temperature and ambient pressure were conducted on stainless steels that were exposed to simulated seawater conditions. Both annealed and hardened conditions were tested and evaluated during aforementioned tests. Preliminary salt solution spray tests have indicated that 2205 duplex stainless steel, 17-7 and 15-5 stainless steels have better corrosion resistance than other alloys in annealed condition. A series of electrochemical impedance spectroscopy (EIS) and cyclic polarization (CP) measurements were conducted on duplex 2205 stainless steel, 17-7 and 15-5 stainless steel in order to evaluate their corrosion resistance both in annealed and hardened conditions. The mechanisms that lead to changes in corrosion resistance due to heat treatment processes are discussed.

3.2 Introduction

Stainless steels are extensively used in various industries due to their good corrosion resistance and mechanical properties [1]. Duplex stainless steels have a two-phase microstructure consisting of ferritic and austenitic phases. Duplex stainless steels have

excellent corrosion resistance and high impact toughness [2]. Precipitation-hardened alloys contain chromium and nickel to optimally combine the properties of martensitic and austenitic grades [3]. Nickel-based alloys generally contain high composition of nickel and some chromium, and they are used for their outstanding corrosion resistance at high temperature [4, 5].

Heat treatment is an effective way to enhance stainless steels' mechanical properties, but it might have some adverse impacts on their corrosion resistance as well. In order to investigate the influence of heat treatment on corrosion resistance of various stainless steels, a series of experiments were conducted. This research was divided into two phases. The first phase consisted of a preliminary study to compare various stainless steels via salt solution spray tests and mechanical properties ranking. The second phase included advanced benchtop electrochemical experiments on selected alloys from phase 1.

3.3 PHASE 1: Preliminary Investigation

The main objective of Phase 1 was to compare various stainless steels with respect to their corrosion resistance and mechanical strengths before quantitative electrochemical tests could be performed on the alloys that show superior performance. The alloys that were investigated included stainless steels (SS), duplex stainless steels (DSS), precipitation-hardened alloys (PHA), and nickel-based alloys (NBA), which have the potential to show good corrosion resistance and mechanical strength in various conditions and applications. The list of alloys and their chemical compositions studied in Phase 1 are provided in Table 3.1.

Table 3.1 Chemical composition (wt. %) of alloys investigated in Phase 1

Type	C	Mn	P	S	Si	Cr	Ni	Cu	Mo	N	Cb	Fe	Other
DSS 2101 (DSS)	0.022	4.82	0.025	0.001	0.68	21.59	1.51	0.39	0.17	0.22	0.008	Bal.	Co: 0.04; Ti: 0.008; Al: 0.009; Sn: 0.002; Ta: 0.002; Pb: 0.001
DSS 2205 (DSS)	0.017	1.49	0.025	0.001	0.31	22.4	5.72	-	3.13	0.17	-	Bal.	-
17-4 (PHA)	0.04	0.5	0.025	0.001	0.2	15.47	4.8	3.27	0.2	-	0.26	Bal.	Ta: 0.10
316 (SS)	0.0161	1.1213	0.029	0.0012	0.2345	16.562	10.015	0.52	2.021	0.0646	-	Bal.	Co: 0.445
AL-6XN (SS)	0.015	0.51	0.029	0.0001	0.35	20.68	23.82	0.37	6.17	0.21	-	Bal.	-
ATI 347 (SS)	0.05	1.17	0.032	0.0002	0.51	17.41	9.1	0.38	0.36	-	0.62	Bal.	-
IN 600 (NBA)	0.02	0.79	0.005	0.0005	0.15	16.31	73.95	0.07	-	-	0.02	Bal.	Co: 0.04; Ti: 0.55; Al:0.24; Ta: 0.002
ATI 800H (NBA)	0.07	0.57	0.01	0.0002	0.32	20.51	30.3	0.04	-	0.011	-	Bal.	Co: 0.04; Ti: 0.55; Al: 0.50
17-7 (PHA)	0.08	0.85	0.023	0.0001	0.34	16.82	7.27	0.25	0.18	0.017	0.014	Bal.	Co: 0.073; Ti: 0.079; Al: 1.07; W: 0.025; V: 0.085; B: 0.0015
15-5 (PHA)	0.04	0.66	0.023	0.001	0.33	15.17	4.3	3.36	0.12	-	0.32	Bal.	Ta: 0.001
ELMAX (SS)	1.7	0.3	-	-	0.8	18.0	-	-	1.0	-	-	Bal.	V: 3.0
M390 (SS)	1.90	0.3	-	-	1.7	20.0	-	-	1.0	-	-	Bal.	V: 4.0 W: 0.60

3.3.1 Experimental Procedure

3.3.3.1 Salt Fog Test

The alloys were studied under salt spray (fog) as per the ASTM B117 [6] standard practice, which provides a controlled corrosive environment that has been utilized to produce relative corrosion resistance information for metal specimens and coated metals exposed in a given test chamber. It should be noted that the prediction of performance in natural environments has seldom been correlated with salt spray results when used as stand-alone data. In this work, we use salt spray (fog) test as a tool to down-select candidate alloys for more detailed and advanced electrochemical testing for corrosion performance.

The salt spray tests were performed using the cyclic corrosion tester [7], which is compliant with ASTM B117 Standard Practice for Operating Salt Spray (Fog) Apparatus. The apparatus consists of a fog chamber, a salt solution reservoir, a supply of suitably conditioned compressed air, one atomizing nozzles, specimen supports, provision for heating the chamber, and necessary means of control. The chamber allows programming of the exposure conditions (spray pressure, relative humidity, temperature, etc.) so that manual intervention is minimized.

A total of 12 candidate alloys (see Table 3.1) with three replicates for each alloy tested in the salt spray chamber for up to 10 days. All alloys samples were cut in a horizontal band saw to a rectangular shape with 3"x 5" dimensions. Elmax and M390 surfaces were grinded by sandpaper due to existing surface oxide layers. The surfaces of other

alloys were not modified. All samples were cleaned by acetone and submerged into a 5wt.% acetic acid ultrasonic bath for 5 minutes, followed by cleaning with deionized water, before they were stored in a desiccator until salt spray testing. Before the salt spray test, all candidate alloy samples were weighted on a top-loading scale, and all dimensions were measured by a digital caliper. Each sample was photographed prior to the experiment. For testing, candidate alloys were placed on racks in the chamber as show in Figure 3.1.

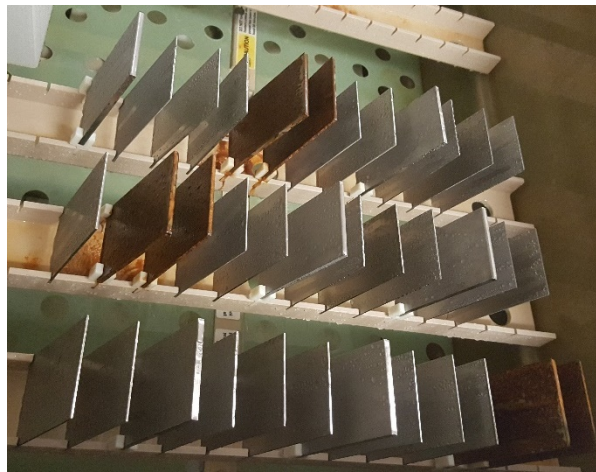


Figure 3.1 Test samples in the corrosion chamber

The salt solution was prepared by dissolving 5 parts by mass of sodium chloride in 95 parts of water conforming to Type IV water in the ASTM Specification D1193 [8]. The salt used was sodium chloride with not more than 0.3 % by mass of total impurities and followed ASTM B117 limitations. When atomized at 35°C the collected solution was in the pH range from 6.5 to 7.2 at 23±3°C. No pH adjustment was deemed necessary for the duration of the test, which was performed at 35°C ±2°C for 10 days. The salt spray pressure was 10-15 psi.

3.3.3.2 Mechanical Properties Ranking

Figure 3.2 shows the Brinell hardness values of the candidate alloys in annealed and hardened conditions [9]. It is clear from the figure that precipitation hardened alloys 17-7, 15-5, and 17-4, as well as duplex stainless steel 2205 have high hardness values in hardened conditions. All these candidate alloys have greater than 15 wt.% chromium and 4-5wt% nickel.

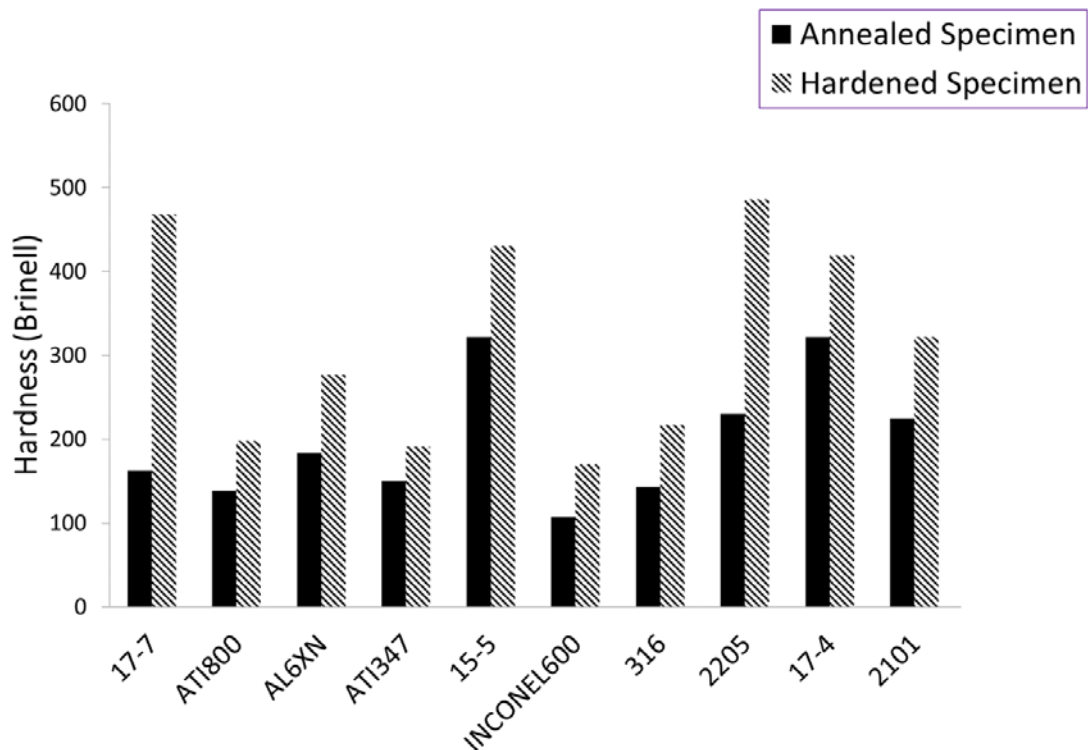


Figure 3.2 Hardness data of candidate alloys

In addition, their hardness is relatively low in the annealed condition, but they have high hardness after heat treatment; the big difference of hardness in these conditions would cause a hardness variance between wrought and final conditions. For wrought alloy, low hardness would make manufacturing process (e.g. stamping, machining, etc.) easier. For the final condition, high hardness is desired for a longer service life.

As a result, 2205, 17-7 and 15-5 alloys were identified for the second phase for more detailed quantitative analysis. Alloy 17-4 was eliminated due to small difference of hardness between annealed and heat treated conditions.

3.3.2 Preliminary Investigation Results

During the daily inspection of samples in the corrosion chamber, it was observed that ELMAX and M390 tool steel alloys (shown in Figure 3.3). Therefore, they were removed from the chamber early, after 4 days of exposure. Other samples were kept in the chamber for the full 10 days. Table 3.2 shows the experiment duration for each candidate alloy type.

Table 3.2 Experiment duration in salt spray tests

Candidate alloys	DAY 2	DAY 4	DAY 7	DAY 10
Duplex stainless steel 2205	X	X	X	X
Stainless steel 17-4	X	X	X	X
Stainless steel 316	X	X	X	X
Stainless steel AL6XN	X	X	X	X
Duplex stainless steel 2101	X	X	X	X
Stainless steel 17-7	X	X	X	X
Stainless steel ATI800	X	X	X	X
INCONEL600	X	X	X	X
Stainless steel 15-5	X	X	X	X
Stainless steel ATI347	X	X	X	X
Tool steel ELMAX	X	X		
Tool steel M390	X	X		

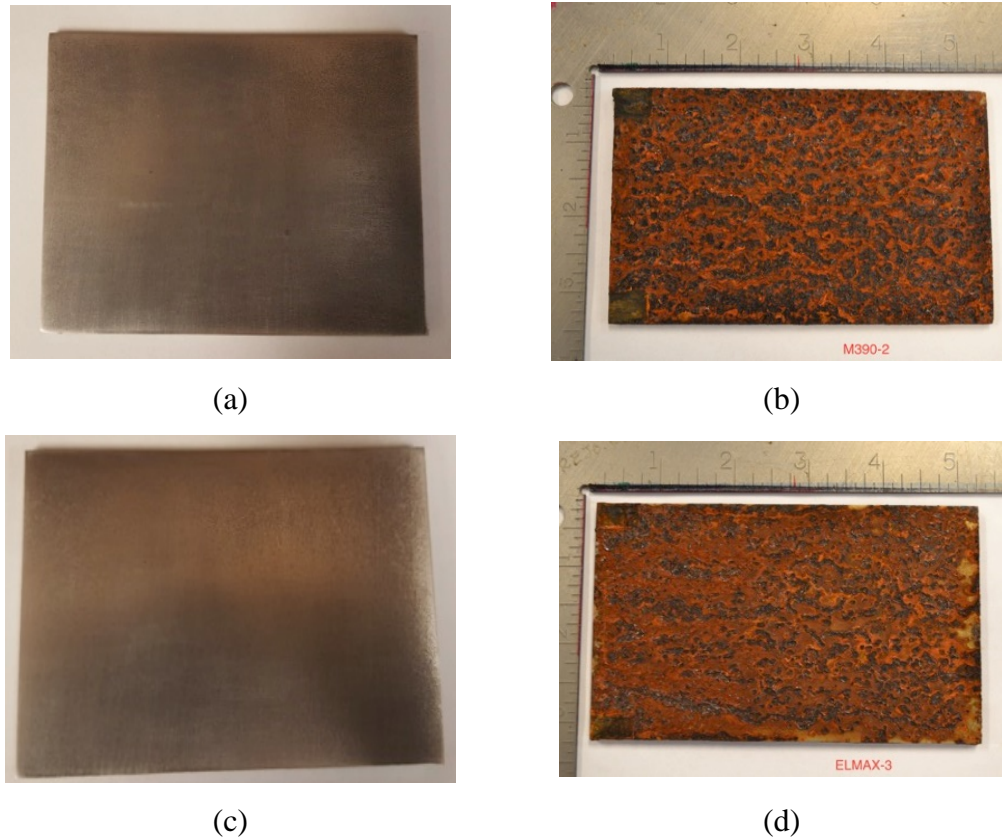


Figure 3.3 Corrosion performance in salt spray test: (a) M390 alloy before exposure, (b) M390 alloy after 4 days of exposure, (c) ELMAX alloy before exposure, (d) ELMAX alloy after 4 days of exposure

All other alloys performed well with little to no signs of corrosion; therefore, no effort was made to quantitatively compare the alloys with respect to their mass loss data. Table 3.3 shows the performance of each alloy, ranged from good (samples with no signs of corrosion), medium (samples with small and superficial pitting), and poor (samples with extensive corrosion, as shown in Figure 3.3). It is clear from Table 3.3 that alloys with both chromium and nickel performed better than stainless steels with chromium only. In general, the higher the nickel plus chromium content, the better corrosion resistance. This trend hold for all alloys except for 347 SS.

Table 3.3 Corrosion test results

Alloys	Corrosion resistance	Cr & Ni concentration
2205	Good	Cr:22.4, Ni: 5.72, total: 28.12
17-4	Good	Cr: 15.47, Ni: 4.8, total: 20.27
316	Good	Cr: 16.56, Ni: 10.11, total: 26.67
AL6XN	Good	Cr: 20.68, Ni: 23.82, total: 44.5
17-7	Good	Cr:16.82, Ni: 7.27, total: 24.09
ATI800	Good	Cr: 20.51, Ni: 30.3, total: 50.81
INCONEL600	Good	Cr: 16.31, Ni: 73.59, total: 89.9
2101	Medium	Cr: 21.59, Ni: 1.51, total: 23.1
15-5	Medium	Cr: 15.17, Ni: 4.3, total: 19.47
ATI347	Medium	Cr: 17.41, Ni: 9.1, total: 26.51
ELMAX	Poor	Cr: 18.00
M390	Poor	Cr: 20.00

3.4 PHASE 2: Corrosion Resistance Investigation of Selected Alloys in Different Heat Treatment

The down-selected alloys from Phase 1 were further investigated through electrochemical and mechanical tests in annealed and heat-treated conditions. Electrochemical tests consisted of open-circuit potential monitoring (OCP), electrochemical impedance spectroscopy (EIS), and Cyclic Polarization (CP).

3.4.1 Materials and methods

As-received 2 mm thick disc samples were cut out of down-selected alloys. After cutting to size, the samples were cleaned with acetone to remove machining greases and oils and rinsed with deionized water. The samples were then immersed in an ultrasonic bath of 5% acetic acid solution, followed by a second rinsing with deionized water. Next, the samples were ground with progressively increasing grit sizes, followed by a polish to 0.05 microns using silica polish. This gave the samples a mirror finish with no noticeable scratches or blemishes. The samples were then rinsed with distilled

water, dried with a delicate task wipe, and then immediately placed into a desiccator with silica desiccant gels until further testing.

As shown in Figure 3.4, a three-probe electrochemical cell was used for electrochemical testing. A Gamry Reference 3000 potentiostat/frequency response analyzer (FRA) was used for taking all electrochemical measurements. Gamry Echem software was used for analyzing impedance data. A graphite counter electrode with a high surface area and an Accumet saturated calomel reference electrode (SCE) were used in all electrochemical measurements. The tip of the reference electrode was placed approximately 5 mm from the surface of the sample.

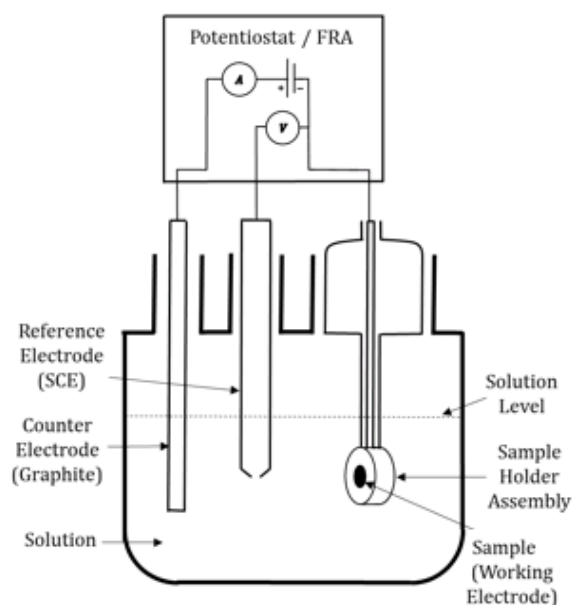


Figure 3.4 Schematic electrochemical test cell

Each sample was loaded into the Princeton Applied Research K0105 sample holder, which is designed for performing repeatable and reliable electrochemical

measurements on one of the exposed cut and prepared surfaces. The sample holder had hydrophobic Teflon washers to protect the sample edges from crevice corrosion; no crevice corrosion was observed in the tested samples during experiments. The exposed surface area after the sample was loaded into the holder was 1 cm². The total resistance of the sample holder assembly was less than 1 Ω . The sample holder was immersed in a 1 L electrochemical cell with separate ports for reference and counter electrodes. The electrolyte used in the electrochemical tests was 3.5% NaCl solution (pH = 7.2), which was prepared by reagent grade NaCl and deionized water. Since CP test is destructive, they were performed as the last test after EIS scans, following ASTM G61 standards (10).

3.4.2 Heat treatment

The heat treatment process for each alloy is described below.

17-7 stainless steel:

- Annealing: Heating to 1950°F and soaking for 1 hour, followed by furnace cooling to room temperature
- Austenite conditioning: Heating to 1750°F soaking for 10 minutes, followed by air cooling to room temperature. Within 1 hour, start cooling to -100F, soaking for 8 hours, then air warm to room temperature.
- Precipitation hardening: Heating to 950°F \pm 10°F, soaking for 1 hour followed by air-cooling to room temperature.

15-5 stainless steel:

- Annealing: Heating and soaking the sample at $1900^{\circ}\text{F} \pm 25^{\circ}\text{F}$ for 1 hour followed by air cooling to room temperature.
- Precipitation hardening: Heating to $900^{\circ}\text{F} \pm 10^{\circ}$ soaking for 1 hour followed by air cooling to room temperature.

2205 duplex stainless steel:

- Annealing: Heating to 1900°F , and then keeping the sample in the furnace for one hour.
- Quenching: Rapidly water cooling
- Aging: Soaking 600°F for one hour.

3.4.3 Electrochemical Test Results

Figure 3.5 shows the bode plots (impedance and phase angle) of EIS experiments performed after samples were exposed to the NaCl solution for 30 minutes. The phase angle at mid frequency range (102-101 Hz) indicate all alloys show passivating trends, possibly due to the presence of chromium in the alloy composition, which thermodynamically favors passive film formation at near neutral pH conditions. As shown in these figures, annealed samples show higher impedance at lower frequencies and more negative phase angles in mid-frequency range than the heat-treated samples. This shows that annealed alloys have higher corrosion resistance in the NaCl electrolyte than the heat-treated alloys. This behavior is attributed to lesser grain boundary area (low energy region) in annealed samples as compared to hardened alloys. After 30

minutes of exposure, as shown in Figure 3.5, annealed alloys 17-7 and 2205 show clear signs of passive behavior, as indicated by phase angles in mid-frequency range approaching -90° and relatively high values of impedance (105-106 ohms) at low frequencies. Annealed alloy 2205 shows slightly better passivation characteristics than annealed alloy 17-7; however, both alloys show considerably more stable passivity than alloy 15-5, as evidenced by relatively high phase angles in the mid-frequency range.

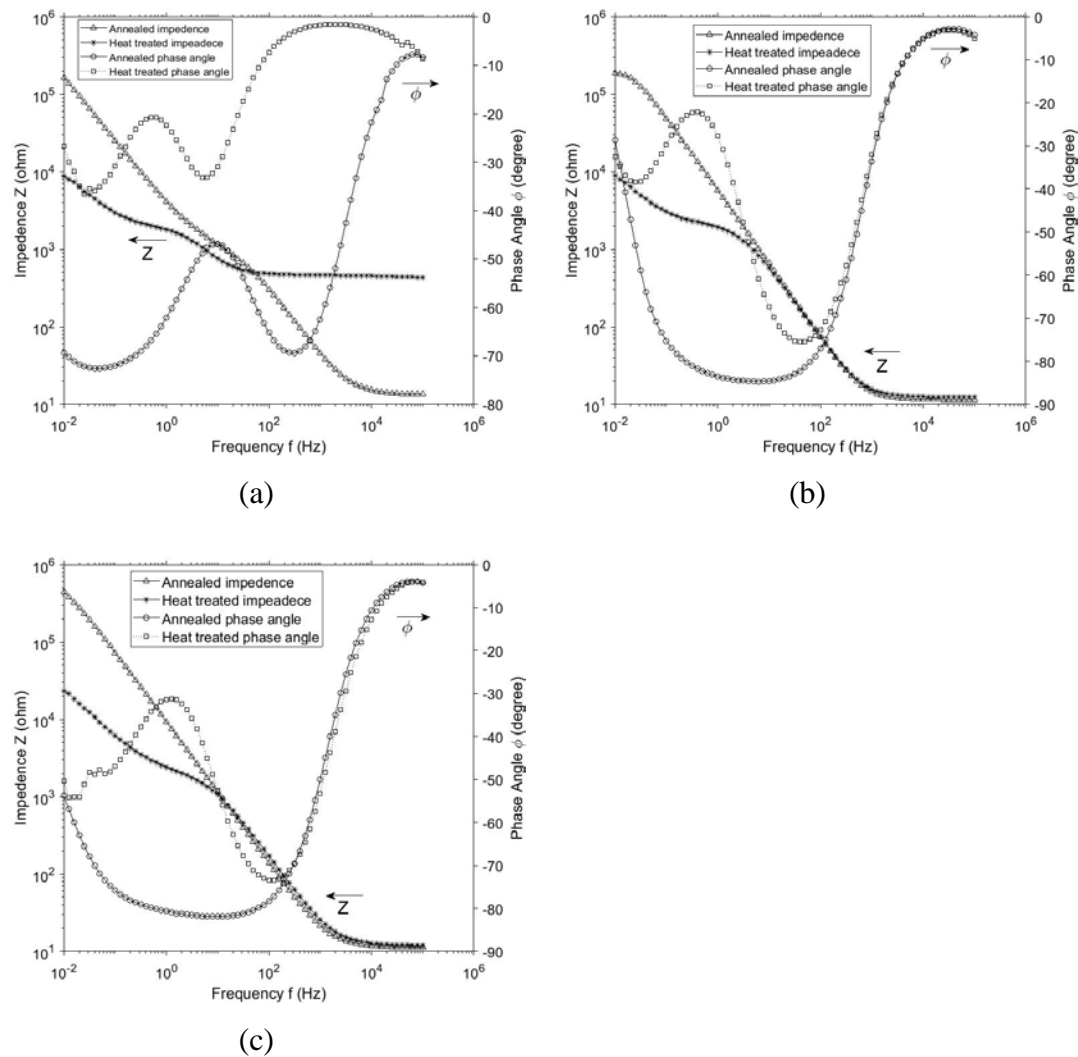


Figure 3.5 Bode plots (impedance and phase angle) for (a) 15-5 (b) 17-7 (c) 2205 stainless steels

CP scans are shown in Figure 3.6. All heat-treated alloys showed pitting behavior. Annealed 15-5 and 17-7 alloys also showed pitting behavior; however, annealed 2205 alloy passivated during increased anodic polarization. CP tests demonstrate the annealed 2205 has the highest resistance to corrosion in the tested NaCl solution.

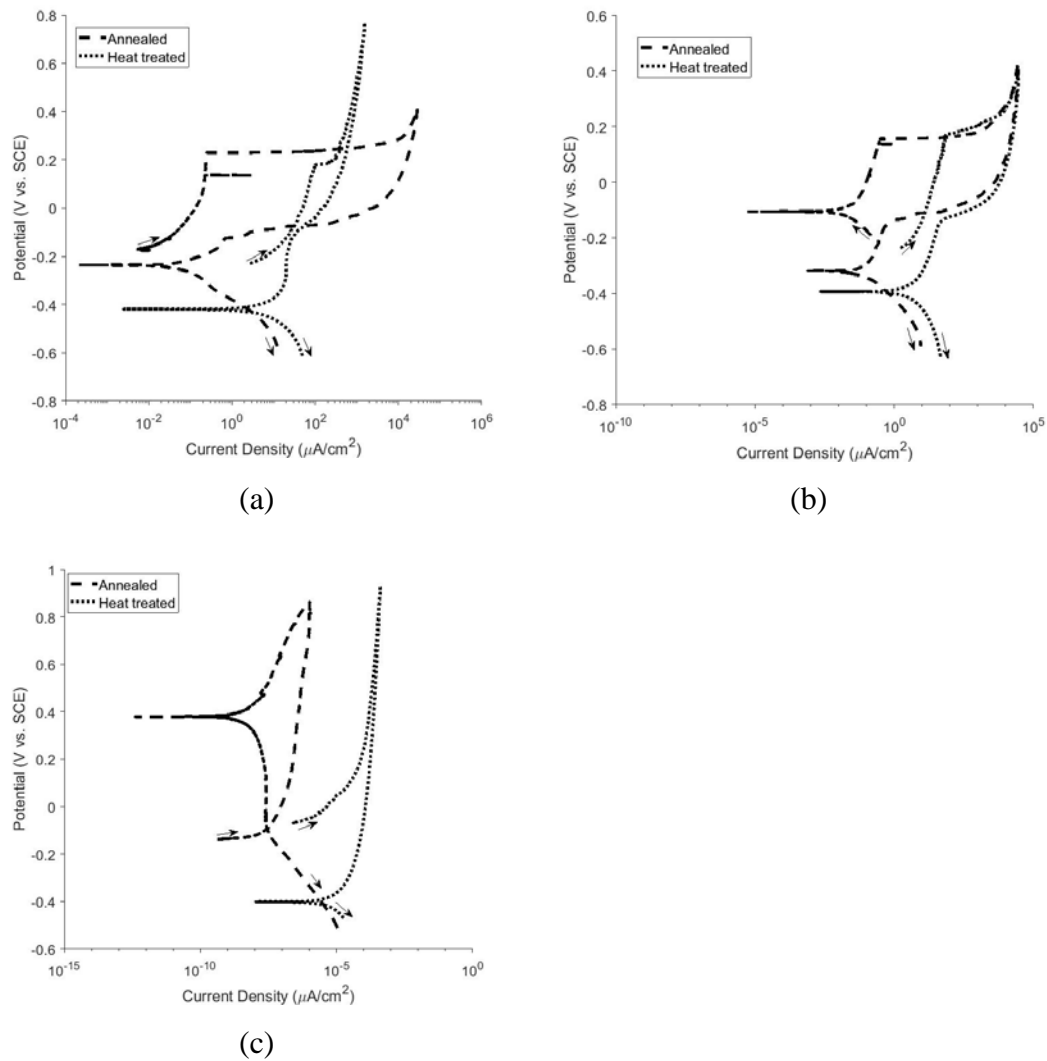


Figure 3.6 Cyclic polarization plots for (a) 15-5 (b) 17-7 (c) 2205 stainless steels

Figure 3.7 presents the CP plots for annealed and heat-treated samples, respectively. In these plots, it is clear that annealed 2205 alloy show the best corrosion performance among the down-selected alloys in both annealed and heat treated conditions.

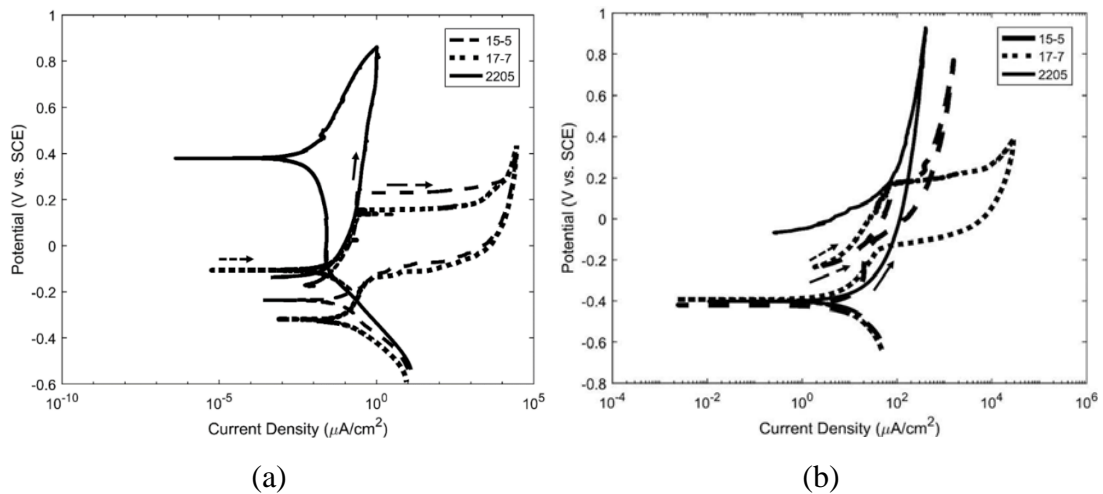


Figure 3.7 Cyclic polarization data for (a) annealed alloys (b) heat-treated alloys

3.5 Conclusion

From phase 1 results, alloys 15-5, 17-7, and 2205 showed the highest performance on corrosion resistance and hardness. After the investigation on the impact of heat treatment through electrochemical experiments, alloy 2205 showed the highest corrosion resistance in annealed and heat treated conditions. Although the corrosion resistance decreased during the heat treatment, it is sufficient compared with other down selected alloys. Alloys 15-5 and 17-7 have decent corrosion resistance and mechanical properties, but 2205 has the best properties overall.

3.6 References

- [1] R. Eluri, and B. Paul, *Journal of Manufacturing Processes*, 14(4): p. 471-477. (2012).

- [2] Solomon, H.D. and T. Devine Jr. Duplex Stainless Steels--A Tale of Two Phases. in Duplex stainless steels. (1982).
- [3] H. Mirzadeh, and A. Najafizadeh, Aging kinetics of 17-4 PH stainless steel. Materials chemistry and physics, 116(1): p. 119-124. (1996).
- [4] M. G. Burke, W.J. Mills, and R. Bajaj. Microstructure and Properties of Direct-Aged Alloy 625. in TMS. (2001).
- [5] R. Bajaj, et al., Irradiation-Assisted Stress Corrosion Cracking of HTH Alloy X-750 and DA Alloy 625. in NACE. (1995).
- [6] ASTM B117, "Standard practice for operation salt spray (fog) apparatus". ASTM International (1997).
- [7] Q-LAB Q-Fog Cyclic Corrosion Testers. (2017). Available from: <http://www.q-lab.com/products/q-fog-cyclic-corrosion-chamber/q-fog-ssp-cct>.
- [8] ASTM D1193, "Specification for Reagent Water". ASTM International. (2011).
- [9] ASM Alloy Center Database, A. International, Editor. (2017).
- [10] ASTM G61 "Standard Test Method for Conducting Cyclic Potentiodynamic Polarization Measurements for Localized Corrosion Susceptibility of Iron-, Nickel-, or Cobalt-Based Alloys". ASTM International. (2014).

4 Corrosion Behavior of Steels in Supercritical CO₂ for Power Cycle Applications

4.1 Abstract

In order to understand issues with corrosion of heat exchanger materials in direct supercritical carbon dioxide (sCO₂) power cycles, a series of autoclave exposure experiments and electrochemical experiments have been conducted. Corrosion behaviors of 347H stainless steel and P91 martensitic-ferritic steel in sCO₂ environment have been compared. In autoclave exposure tests performed at 50°C- 245°C and 80 bar. Mass change measurements, surface characterization, and corrosion product analysis have been conducted to understand the corrosion behavior of steels in sCO₂ containing H₂O and O₂. Electrochemical tests performed at room temperature and 50°C, a simulation environment of water condensation phase with dissolved CO₂ was prepared to evaluate the corrosion resistance of materials. From both types of experiments, generally 347H showed higher corrosion resistance than P91.

4.2 Introduction

Supercritical CO₂ has been investigated for use in power cycles. These sCO₂ cycles are projected to have higher efficiencies compared to steam cycles due to reasons such as lack of phase change in working fluid within the working envelope, recompression of sCO₂ near liquid densities, and high heat recuperation. In addition to the higher efficiencies, dry or reduced water cooling in direct and indirect cycles and producing storage ready CO₂ in direct cycles will also lower the environmental impact.

Furthermore, compact turbo machinery and simple configurations of the CO₂ cycles could result in lower capital cost.

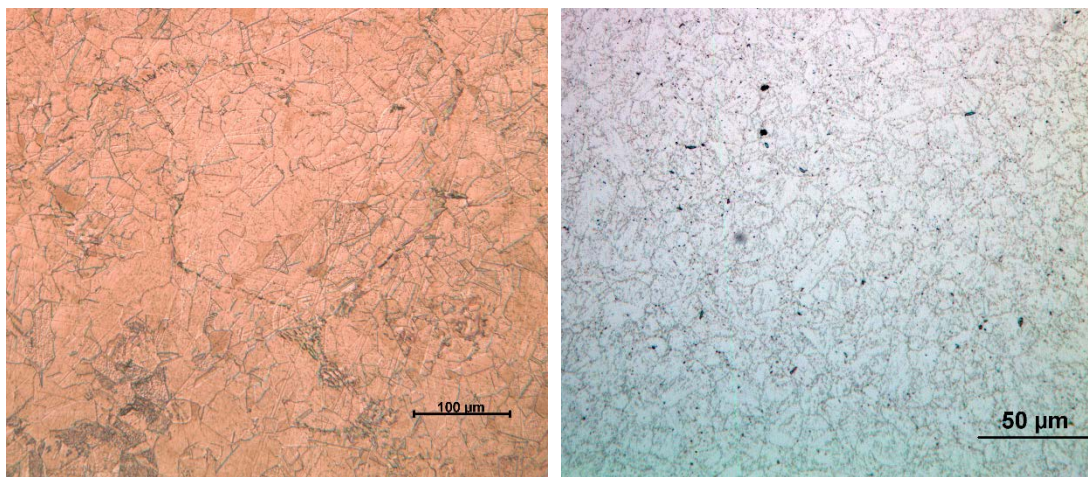
Direct sCO₂ cycle is a process that utilizes pressurized combustion exhaust as working fluid and expands it through a turbine to generate power. The combustion exhaust contains primarily CO₂ in supercritical state with water and O₂ dissolved in it. Depending on the fuel (natural gas, coal derived syngas, etc.), the working fluid may contain other impurities such as SO₂ and HCl [1]. The expanded working fluid goes through heat exchangers to transfer the heat to the incoming high-pressure CO₂ used for dilution in the combustor. Some of the CO₂ is diverted for sequestration after water separation.

Heat exchanger is a key part in direct sCO₂ power cycle. Corrosion resistance of heat exchanger materials is significant for its sustainability. This research is conducted to study the corrosion mechanisms of two alloys, austenitic stainless steel 347H, and martensitic-ferritic steel P91 in sCO₂ containing O₂ and H₂O impurities. The results presented are divided into two parts: autoclave exposure experiments and electrochemical experiments. For the autoclave exposure experiments, the purpose is to evaluate the candidate materials in a simulated heat exchanger environment. The sCO₂ fluid phase contained O₂ and H₂O. The electrochemical experiments were carried out to reveal the corrosion mechanisms and measure the corrosion rates for cases where water saturated with CO₂ condenses on material surface.

4.3 Experimental Procedures

4.3.1 Autoclave Exposure Experiments

Alloy coupons of 347H austenitic stainless steel and P91 martensitic-ferritic steel were machined with a size of 25 x 20 x 6 mm. Chemical compositions of the alloys are shown in Table 4.1. Microstructures for 347H and P91 are shown in Figures 4.1a and 4.1b, respectively, and both show grain boundaries with even grain sizes [2]. All coupons have a 1200 grit SiC paper final surface finish, and have been cleaned prior to experiments. They are exposed to a gaseous phase with a mixture of CO₂:O₂=95:1, which is combined with H₂O in three different conditions as shown in Table 4.2. Each condition has eight samples that were hung on Teflon sleeves in an 1100 ml autoclave.



(a) 347H

(b) P91

Figure 4.1 Microstructures of candidate alloys

Table 4.1 Chemical composition of alloys

Alloy	Description	Cr	Ni	C	Mn	P	S	Si	Co	Cu	Mo	N	Cb	Fe
347H	Austenitic stainless steel	17.3	9.09	0.05	1.5	0.03	0.01	0.38	0.16	0.43	0.41	0.04	0.62	Balance
P91	Martensitic-ferritic steel	8.37	0.09	0.9	0.45	0.01	0.01	0.33		0.09	0.9	0.45	0.07	Balance

Table 4.2 Exposure conditions

Exposure condition	Temperature (°C)	Pressure (bar)	Water Volume (ml)	Time (hours)	Shut down procedure
Condition 1	50	80	400	500	Temperature and pressure drop simultaneously
Condition 2	245	80	6.7	500	Temperature and pressure drop simultaneously
Condition 3	245	80	6.7	500	Pressure drops, and then temperature drops

Exposure conditions are schematically shown in Figure 4.2 [4]. In condition 1, four samples were submerged in water rich phase, while the other four were exposed to sCO₂ -rich phase. Conditions 1 and 2 have the same mole fraction of H₂O in CO₂ in sCO₂ rich phases, which was calculated from H₂O saturated in CO₂ at two different temperatures (3).

Conditions 2 and 3 have an identical environment prior to the end of exposure. The difference between them is H₂O condensation during the shutdown period. Figure 4.3 shows the temperature-pressure profiles. In condition 2, pressure and temperature were gradually lowered simultaneously. In condition 3, pressure was lowered to ambient pressure while the temperature was maintained at 245°C. After the pressure reached ambient pressure, the temperature was lowered to room temperature. As a result, condition 2 has an H₂O condensation period during shutdown, while condition 3 does not.

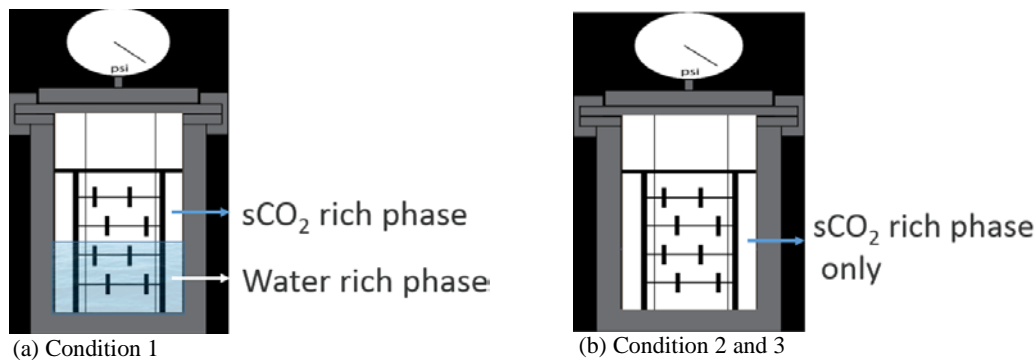


Figure 4.2 Autoclave experiments setup [4]

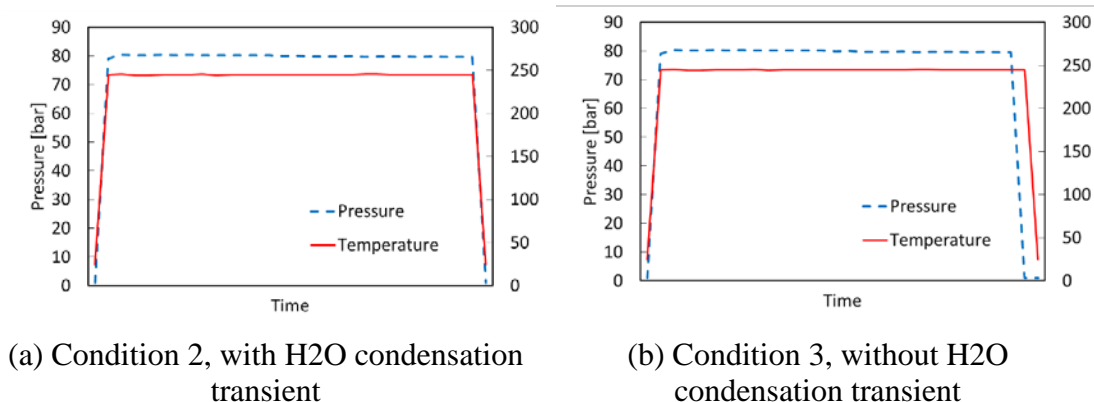


Figure 4.3 Temperature-pressure profile of condition 2 and 3.

4.3.2 Electrochemical experiments

Electrochemical tests were conducted at two different temperatures, 25 and 50°C. Electrolyte was prepared by constantly bubbling CO₂ into deionized water in order to create carbonic acid (5). The pH was measured to ensure a stable solution. As shown in Figure 4.4, pH is 4.1 at 25°C after bubbling CO₂ for 30 minutes, and pH is 4.2 at 50°C after same amount of time. The Counter electrode was Platinum, and the reference electrode was saturated calomel electrode. The same alloy coupons were used as in the autoclave exposure experiments with a 1200 grit SiC paper surface finish. Types of electrochemical experiments performed are as follows:

- Linear polarization resistance, scan rate 0.125 mV/s

- Potentiodynamic scan, scan rate 5 mv/s
- Cyclic voltammetry, scan rate 5 mv/s
- Potentiostatic scan, 300 s

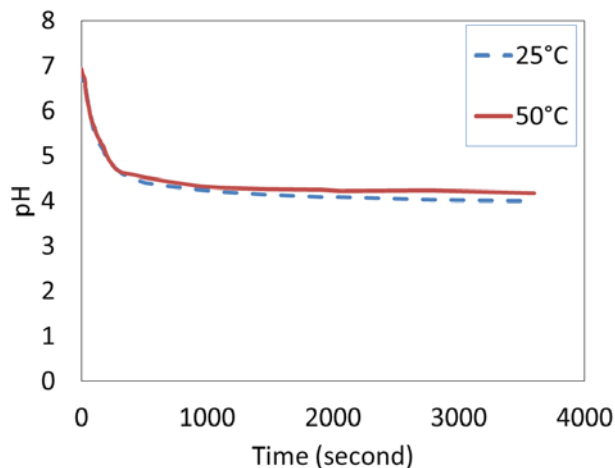


Figure 4.4 pH measurement of electrolyte at 25 and 50°C

4.4 Results and Discussion

4.4.1 Autoclave Exposure Experiments Results

Multiple findings can be concluded from the mass change results in Figures 4.5 and 4.6.

- Figures 4.5 and 4.6 show that 347H has less mass change than P91 in all conditions, which demonstrates that 347H is more corrosion resistant than P91 in the exposure environments.
- As showed in Figure 4.5, the coupons in H₂O rich phase experienced a negative mass change due to the dissolution of corrosion products into aqueous phase. P91 has a large error bar in CO₂ rich phase, because the coupons close to the water surface have corrosion product dissolved into

water due to water splash during startup period, while the ones farther from the water surface have less influence from water splash. Because of this error, the comparison of corrosion resistance between CO₂ and H₂O rich phases needs to be determined by mass loss and corrosion rate calculation.

- As can be seen in Figure 4.6, the coupons in condition 3 showed less mass change than the ones in condition 2, which demonstrates that H₂O condensation is the main cause of corrosion.

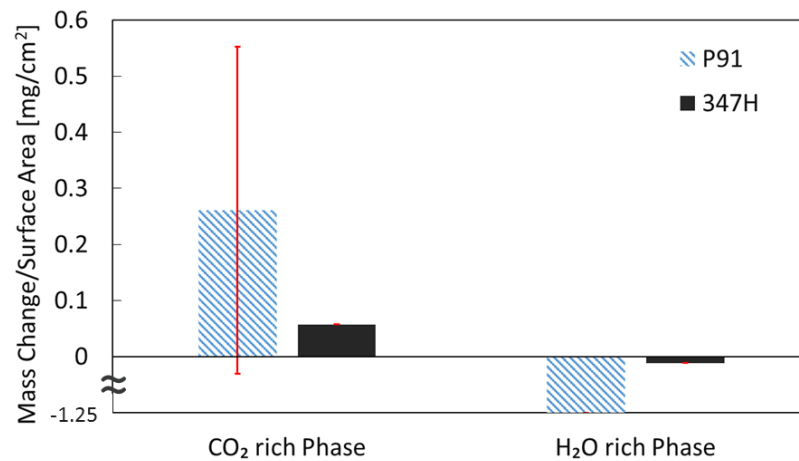


Figure 4.5 Mass change comparison as a function of phases at 50°C and 80 bar in condition 1.

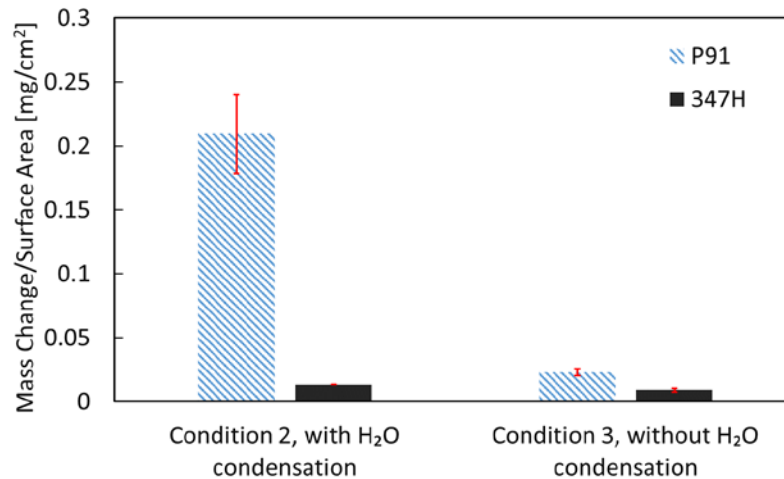


Figure 4.6 Mass change comparison of condition 2 and 3, as a function of Water condensation at 245°C and 80 bar in CO₂ rich phase

Sample surfaces were characterized by X-ray diffraction for coupons in conditions 1 and 2. The corrosion product layer formed on the 347H sample surface was too thin to be detected. Also, 347H has less than 0.05 mg/cm² mass change over all. Table 4.3 shows that on the P91 iron hydroxide products formed, but no iron carbonates. This phenomenon shows the dominant species affecting corrosion mechanisms are oxygen and water. Figure 4.7 shows P91's images after autoclave exposure. In conditions 1 and 2, coupons have obvious corrosion products on surfaces, while condition 3 coupons have relatively clean surfaces, which is verified by mass change results that condition 3 samples have the least mass change.

Table 4.3 Glancing angle XRD results of corrosion products

Alloys	Condition 1		Condition 2	Condition 3
	sCO ₂ rich phase	H ₂ O rich phase	sCO ₂ rich phase	sCO ₂ rich phase
347H	Base metal	Base metal	Base metal	TBD
P91	Hematite(Fe ₂ O ₃) Base Metal	Hematite(Fe ₂ O ₃) Magnetite(Fe ₃ O ₄) Goethite(FeO(OH))	Goethite(FeO(OH)) Base Metal	TBD

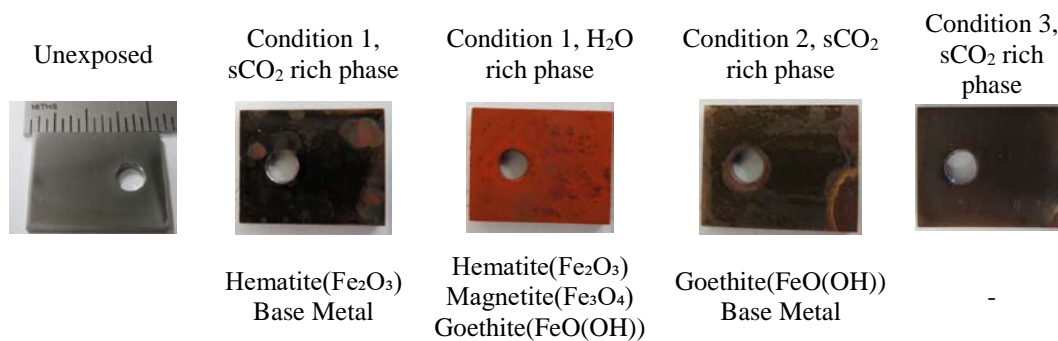
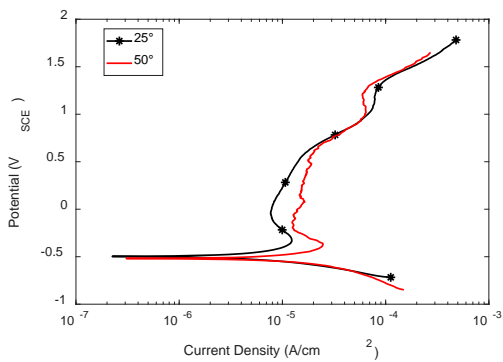


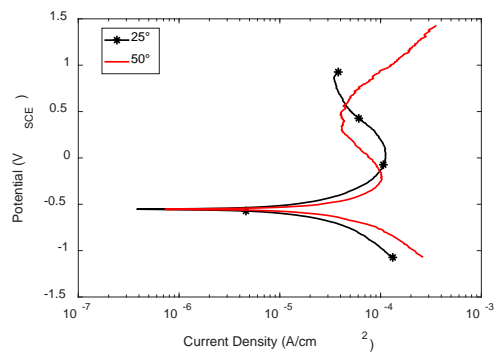
Figure 4.7 P91 coupon images after autoclave exposure experiments

4.4.2 Electrochemical experiments results

Results of the electrochemical experiments are shown in Figures 4.8 through 4.12. From potentiodynamic polarization scans, alloys' anodic and cathodic parts have similar characteristics. The plots in Figure 4.8 both display the following regions: cathodic, active, active-passive, passive, and transpassive. Also, they both have higher corrosion current density at higher temperature extrapolated from Tafel slopes. Linear polarization resistance scans verified the same conclusion that alloys have higher corrosion current density at 50°C. Cyclic voltammetry demonstrates that P91 is prone to localized corrosion as pitting corrosion indicated from the curves at both temperatures. Potentiostatic polarization scans were conducted at primary passivation potentials selected from the potentiodynamic polarization curves for both alloys at each temperature. Potentiostatic scans prove that 347H starts passivation ahead of P91.

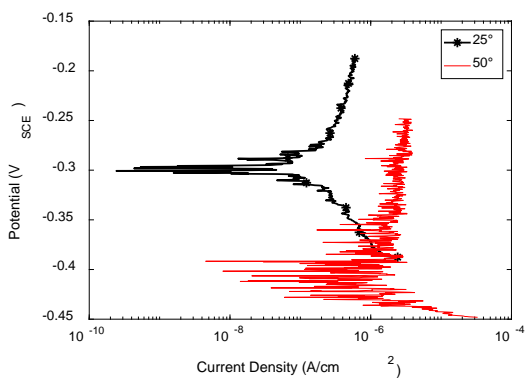


(a) 347H

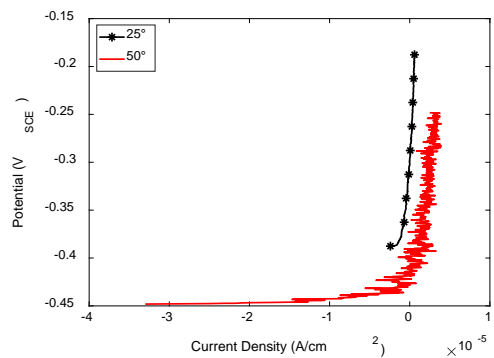


(b) P91

Figure 4.8 Potentiodynamic polarization scans

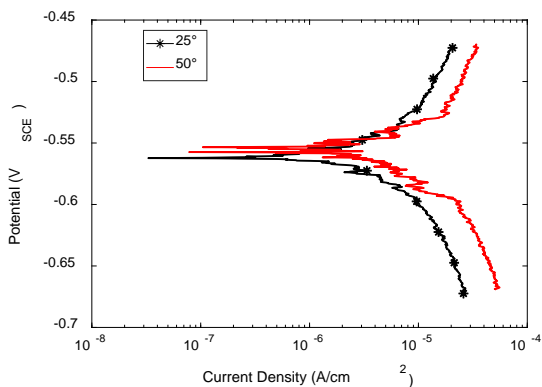


(a) Logarithmic scale

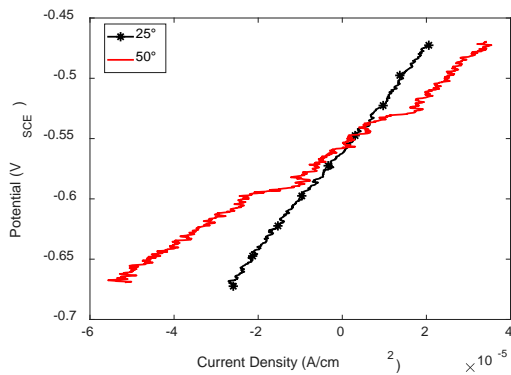


(b) Linear scale

Figure 4.9 347H linear polarization resistance



(a) Logarithmic scale



(b) Linear scale

Figure 4.10 P91 linear polarization resistance

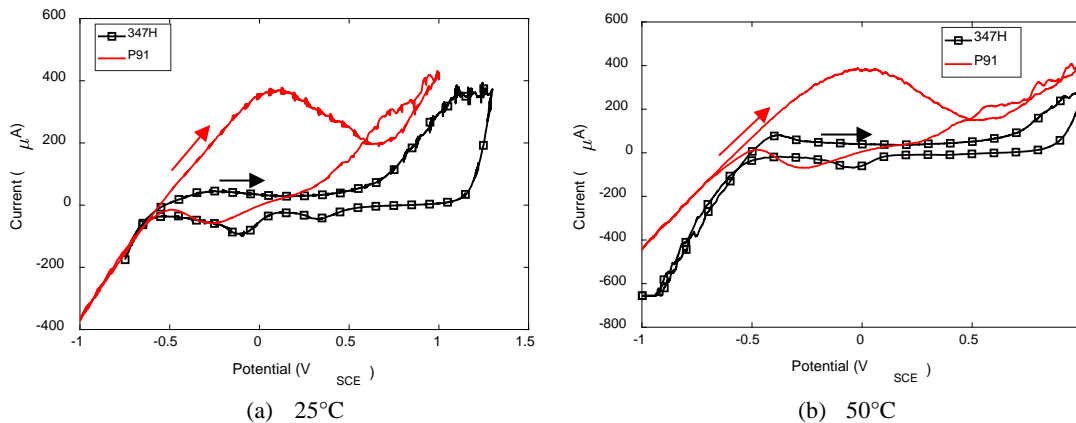


Figure 4.11 Cyclic voltammetry scan

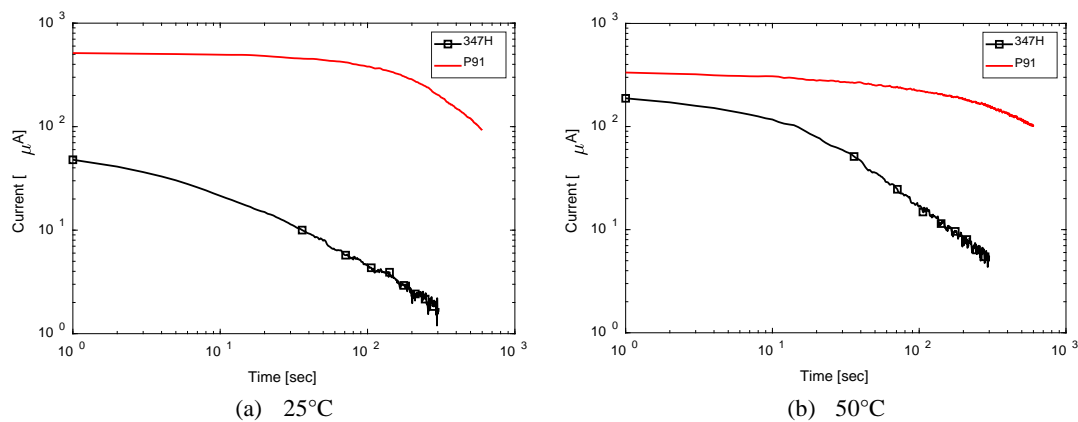


Figure 4.12 Potentiostatic polarization scan

4.4.2.1 Corrosion rate calculations

All corrosion rates were calculated from equations 1 through 6 (6 to 8). As demonstrated from the corrosion rates of potentiodynamic scan and polarization resistance, both alloys have higher corrosion rate at higher temperature; furthermore, P91 has higher corrosion rate than 347H. The discrepancy of corrosion rate results between potentiodynamic scan and linear polarization is due to the large difference of scan rates. Potentiodynamic scan has a 5 mv/s scan rate, while linear polarization resistance has a 0.125 mv/s scan rate.

$$\eta_c = -\frac{2.3RT}{\alpha nF} \log \frac{i_c}{i_0}, \beta_c = -\frac{2.3RT}{\alpha nF} \quad (\text{Eq. 4.1})$$

$$\eta_a = \frac{2.3RT}{\alpha nF} \log \frac{i_c}{i_0}, \beta_a = \frac{2.3RT}{\alpha nF} \quad (\text{Eq. 4.2})$$

$$i_a = i_c = i_{corr} \quad (\text{Eq. 4.3})$$

$$\text{Corrosion Rate} = K_1 \frac{i_{corr}}{\rho} EW \quad (\text{Eq. 4.4})$$

$$\text{Stern Geary Equation: } i_{corr} = \frac{B}{R_p} \quad (\text{Eq. 4.5})$$

$$\text{Stern Geary Constant : } B = \frac{\beta_a \beta_c}{2.303(\beta_a + \beta_c)} \quad (\text{Eq. 4.6})$$

Table 4.4 Corrosion rates

Alloy and Temperature	Potentiodynamic Polarization, Scan Rate 5 mv/s		Polarization Resistance, Scan Rate 0.125 mv/s		
	Corrosion Current Density [$\mu\text{A}/\text{cm}^2$]	Corrosion Rate [mm/year]*	Rp [Ω/cm^2]	Corrosion Rate [mm/year]*	Corrosion rate [mm/year]**
347H at 25°C	2.73	2.83×10^{-2}	2.47×10^4	2.74×10^{-2}	1.04×10^{-2}
347H at 50°C	5.81	6.03×10^{-2}	2.01×10^4	3.52×10^{-2}	1.44×10^{-2}
P91 at 25°C	4.71	5.26×10^{-2}	8.43×10^2	6×10^{-1}	1.70×10^{-1}
P91 at 50°C	9.94	11.1×10^{-2}	4.75×10^2	7.2×10^{-1}	3.27×10^{-1}

*Corrosion rate determined from Tafel slopes

**Corrosion rate determined from Stern Geary Equation

4.5 Conclusions

Multiple conclusions can be made from the autoclave and electrochemical experiments.

- The electrochemical experiments show that corrosion rate for each candidate alloy increases as temperature increases, which is in good agreement with kinetic predications.
- Both the autoclave and electrochemical test results prove that 347H has better corrosion resistance than P91. 347H has less mass change than P91 in all autoclave exposure tests. The electrochemical corrosion rate calculations demonstrate that 347H has lower corrosion rate than P91
- Based on the cyclic voltammetry results, P91 is susceptible to localized corrosion.
- As demonstrated from the composition of conditions 2 and 3, corrosion mostly happens when water is present in liquid form. Thus, this conclusion can be extrapolated to sCO₂ cycles: aqueous corrosion mostly happens during the shutdown period when water condenses.

4.6 Acknowledgments

This work was performed in support of the U.S. Department of Energy's Fossil Energy (FE) Crosscutting Technology Research Program. This research was supported in part by appointments (RR and LT) to the National Energy Technology Laboratory Research Participation Program sponsored by the U.S. Department of Energy and administered by the Oak Ridge Institute for Science and Education. The authors would like to thank the following people for their hard work and contribution to this project: Mr. Jeffrey Oberfoell, Dr. Randal Thomas, Dr. Richard Oleksak, Dr. Nicolas Huerta, Dr. John Baltrus, Dr. Alvaro Rodriguez, and Dr. Monica Kapoor, all with NETL.

Discussions with 8 Rivers Capital personnel about direct supercritical CO₂ power cycles are appreciated.

This report was prepared as an account of work sponsored by an agency of the United States Government. Neither the United States Government nor any agency thereof, nor any of their employees, makes any warranty, express or implied, or assumes any legal liability or responsibility for the accuracy, completeness, or usefulness of any information, apparatus, product, or process disclosed, or represents that its use would not infringe privately owned rights. Reference herein to any specific commercial product, process, or service by trade name, trademark, manufacturer, or otherwise does not necessarily constitute or imply its endorsement, recommendation, or favoring by the United States Government or any agency thereof. The views and opinions of authors expressed herein do not necessarily state or reflect those of the United States Government or any agency thereof.

4.7 References

- [1] X. Lu, IEA Clean Coal Centre, “Novel sCO₂Allam Cycle for High-Efficiency, Low Cost and Emission-free Power Generation,” (2016)
- [2] M. Kapoor, Private Communication, (2017)
- [3] L. Teeter, M.S. Thesis, Materials Science Program, Oregon State Univ., “Corrosion of Carbon and Stainless Steels in H₂O-sCO₂ Environments for Power Cycle Applications,” Corvallis, OR (2016).
- [4] L. Teeter et al., ECS Trans., “Corrosion Behavior of Austenitic Stainless Steel in Supercritical CO₂ containing O₂ and H₂O,” Albany, OR (2016)
- [5] S. Sim et al., Corrosion Vol. 68, No. 4. “Use of Aqueous Solutions to simulate Supercritical CO₂ Corrosion,” Clayton, Australia (2011)
- [6] M. Fontana, McGraw-Hill, Inc. Corrosion Engineering, (1986)
- [7] D. A. Jones, Prentice-Hall. Inc. Principles and Prevention of Corrosion, Upper Saddle River, NJ (1996)

- [8] ASTM G102-89(2015)e1 Standard Practice for Calculation of Corrosion Rates and Related Information from Electrochemical Measurements, ASTM International, West Conshohocken, PA (2015)

5 Conclusion

In this work, the corrosion resistance of several alloys were studied under two different environments, salt water and SCO_2 . Although these two studies have different applications, they share the same focus and analysis methodologies. Using combined corrosion tests can provide more insights about the corrosion behavior of alloys. Exposure tests can provide direct feedback of corrosion products, and it has better correlation with real world environments. Electrochemical tests show the corrosion mechanism, and the corrosion behavior can be controlled during the tests. Both of the methods can give corrosion rate results. However, the correlation between these two tests is an uncertainty, especially when they have dramatically different environments. Therefore, it is recommended that use multiple corrosion tests to evaluate the corrosion resistance of alloys.

Alloy selection is a critical decision for many applications. Typically, high corrosion resistance and mechanical strength alloys have higher prices, such as stainless steels with high Cr, Ni, Mo etc. contents. Also, various heat treatment can cause the change of mechanical strength and corrosion resistance. Therefore, an optimization between the costs, corrosion resistance, mechanical properties, and maintaining of alloys is needed for every alloy industry.

5.1 Investigation of Corrosion Resistance for Annealed and Hardened Stainless Steels

Cr content has the dominant impact on corrosion resistance in salt water environment. High Cr content stainless steels have high corrosion resistance due to the formation of Cr_2O_3 . Thus duplex stainless steel 2205 has the highest corrosion resistance among other alloys, though the corrosion resistance decreased after heat treatment, which concludes that heat treatment may have a negative impact on corrosion resistance.

5.2 Corrosion Behavior of Steels in Supercritical CO_2 for Power Cycle Applications

Stainless steel 347H has better corrosion resistance than martensitic-ferritic steel P91. Electrochemical tests have proven that P91 is prone to localized corrosion and it has higher corrosion rates from linear polarization resistance and potentiodynamic polarization. Autoclave exposure tests also demonstrated that P91 has more corrosion products formed than 347H, and corrosion mostly happened during the condensation for both of the alloys.

6 Suggested Future works

Some suggested future works based on each project are listed below.

6.1 Investigation of Corrosion Resistance for Annealed and Hardened Stainless Steels

Based on the change of corrosion resistance for each alloy after different heat treatment, some suggested future works are listed below:

- In order to deeply understand the correlation between heat treatment and corrosion resistance, various heat treatment can be conducted to increase hardness of alloys while maintain or increase corrosion resistance.
- Based on existing alloys' corrosion resistance, applying coating is an efficient way to improve corrosion resistance in salt water environment. Thus, investigate new coating that have high toughness and corrosion resistance in salt water environments could be beneficial.

6.2 Corrosion Behavior of Steels in Supercritical CO₂ for Power Cycle Applications

Some future works are suggested for the project in order to have a complete database and be able to compare with literature data.

- To find out the most corrosive temperature in autoclave test, more tests at various temperatures need to be done tests in water rich and CO₂ rich phases respectively, as a function of corrosion rate and temperature

- In order to create a better correlation between electrochemical and autoclave tests, we need to conduct electrochemical tests under same similar pressure and temperature as autoclave tests.
- To compare with literature data, complete the rest of the corrosion products characterization and corrosion rate calculation is necessary